MARINE CONTROLLED-SOURCE ELECTROMAGNETIC RESPONSES OF A THIN HYDROCARBON RESERVOIR BENEATH ANISOTROPIC OVERBURDEN

A Thesis

by

SANGSEOK YOUN

Submitted to the Office of Graduate and Professional Studies of
Texas A&M University
in partial fulfillment of the requirements for the degree of

MASTER OF SCIENCE

Chair of Committee,	Mark Everett
Committee Members,	Yuefeng Sun
	Zoya Heidari
Head of Department,	John Giardino

August 2014

Major Subject: Geophysics

ABSTRACT

In many cases of exploration geophysics, isotropic Earth forward models have been developed and measured data can be interpreted by inversion using this class of model. An isotropic model treats the Earth as a simple structure, in which the relevant physical properties do not vary with direction, and the interpretation of the measured responses requires relatively less effort compared to interpretations based on anisotropic models. However, the actual Earth has anisotropic physical properties. Thus, a better understanding of anisotropic Earth responses using the MCSEM method is the main objective of this thesis.

The controlled-source electromagnetic response in the frequency domain due to excitation by a horizontal electric dipole (HED) transmitter is herein evaluated over a layered seafloor consisting of a uniaxial anisotropic layer and an isotropic basement. Nominally, the upper uniaxial layer represents a thin-layered or interbedded earth formation caused by sedimentation over geologic time. Unlike an isotropic layer, a uniaxial layer is characterized by different values of electrical conductivity along two different directions.

To solve the MCSEM forward problem for a uniaxial model with vertical anisotropy, it is required to combine Faraday's law and Ampere's law without displacement current, thereby forming the governing pre-Maxwell's equations. The resulting diffusion equation in the spatial (x, y) domain is converted to horizontal wavenumber (p, q) domain using a 2-D Fourier transform. The solution is analytic in the

case of a uniaxial halfspace. The required source terms from an HED deployed in a conducting isotropic wholespace are derived from the Hertz vector potential and expressed, as usual in this type of problem, by Hankel transforms.

Numerical modeling is required to evaluate MCSEM responses of more complicated Earth models, whether isotropic or anisotropic. Herein, the response of a resistive disk located below a vertical anisotropic layer is considered. This serves to investigate the effect of the anisotropic overburden on resolving the underlying disk. The response of the resistive disk placed beneath the anisotropic layer is finally evaluated using a finite element method implemented in the code SEATEM, which was previously developed by Badea *et al*. (2001).

ACKNOWLEDGEMENTS

I would like to thank Dr. Mark Everett and my committee members Dr. Sun and Dr. Zoya for giving their valuable time, guidance, and opportunity to work on such a fascinating topic.

I also thank my company (Korea Gas Corporation, KOGAS) and the persons concerned for giving me a chance to study at Texas A&M University.

Finally, thanks to my parents, brother and my friends for their patience and persistent love.

NOMENCLATURE

MCSEM	Marine Controlled-source Electromagnetic
HED	Horizontal electric dipole
MT	Magnetotellurics
TX	Transmitter
RX	Receiver
EX	Total electric field response
EX-EX	Total electric field response due to an x-directed HED source
PDE	Partial differential equation
ODE	Ordinary differential equation

TABLE OF CONTENTS

Page

LIST OF FIGURES

Page

LIST OF TABLES

Page

1. INTRODUCTION

1.1 History of electromagnetic exploration

Electromagnetic (EM) geophysics has long been used to investigate the internal structure of the Earth to depths of several km or more. Different types of EM geophysical techniques have been used in many areas such as groundwater resources development, pollution monitoring, and hydrocarbon detection on land. For example, Urengoy gas field, the world's second largest natural gas field located in West Siberia of Russia, was surveyed using the magnetotelluric method (MT) to identify basin structure (Kaufman and Keller, 1983). On the seafloor, the deployment of man-made marine sources in the frequency band 0.1~10Hz (controlled-source electromagnetics; CSEM) was developed by academia in the decades 1980-2000 to study ocean basins and midocean ridges (Chave and Cox, 1982; Chave *et al*., 1991; Constable and Cox , 1996; MacGregor *et al*., 1998; 2001).

The marine CSEM method is closely related to the well logging method. The Schlumbeger brothers (1912) found that surface electric measurements can help to characterize subsurface geologic bodies. The first electrical resistivity well logs were acquired in 1927. Shortly after, Archie (1942) developed an empirical relationship between porosity, electrical conductivity, and brine saturation of clay-free sandstones. This primary petrophysical relationship

$$\rho_{bulk} = \frac{a\,\rho_{water}}{\phi^m S_{water}^n}$$

remains important to understand marine CSEM responses. In the above equation, the quantity ρ_{water} is bulk resistivity, ϕ is porosity, ρ_{water} is water resistivity, S_{water} is water saturation, *m* is the cementation exponent, and *n* is the saturation exponent. Archie's equation shows that water-bearing sediments have relatively low bulk resistivity (high conductivity); on the contrary, hydrocarbon reservoirs have higher bulk resistivity (lower conductivity). Despite the recent surge in application of surface-based EM methods, the most widely used EM method continues to be well loggings.

In 2000, the Norwegian oil company Statoil tested the marine CSEM exploration method for hydrocarbon exploration (Ellingsrud *et al*., 2002), and they detected hydrocarbon reservoirs saturated at 60-70% with high economic value. For reference, the relationship between bulk electrical resistivity, the physical property sensed by MCSEM, and hydrocarbon saturation of a clean hypothetical sandstone reservoir is shown in Figure 1. After these encouraging results, the company ElectroMagnetic GeoServices (EMGS) was established for commercial hydrocarbon exploration using the marine CSEM technique, and EMGS named their method 'sea bed logging'. Shortly after the founding of EMGS, the competitors Offshore Hydrocarbon Mapping (OHM) and AGO/Schlumberger introduced similar methods to explore offshore hydrocarbon reservoirs.

The commercial operations usually employ a horizontal electric dipole source and remote electromagnetic field sensors placed on the ocean floor. The various companies performed more than 100 surveys in the few years after the initial tests, and drilling results confirmed the presence of hydrocarbons in many cases. Major

commercial exploration and production companies such as ExxonMobil, Shell, and BP, along with many national oil and gas companies from different countries worldwide have now successfully used the marine CSEM method, and smaller companies along with university researchers are improving various aspects of the technique.

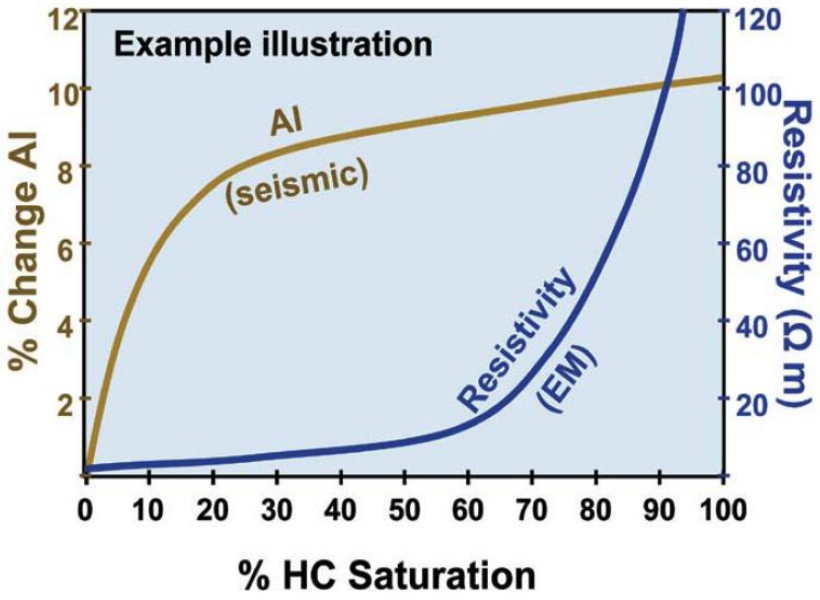

Figure 1. Percentage change in acoustic impedance and the value of bulk resistivity, as functions of the hydrocarbon saturation of a hypothetical clean sandstone reservoir (Hesthammer *et al*. 2010).*

* Reprinted with permission from "CSEM performance in light of well results" by Hesthammer et al, 2010, *The Leading Edge*, 29, No. 1, P.258-264. Copyright 2010 by SEG

1.2 Background of MCSEM

Marine controlled-source electromagnetics (MCSEM) is a geophysical exploration method that can detect electrically resistive zones, such as hydrocarbon reservoirs, beneath the seafloor. In MCSEM, an energy source, or transmitter (TX), is towed by a vessel, as in the marine seismic exploration method. A horizontal electric dipole (HED) transmitter, for example, injects a time-varying primary electric current into the seafloor. The primary EM field diffuses into the Earth. The time variations in the primary field induce electromagnetic eddy currents in the seafloor, which in turn generate a secondary EM field. The eddy currents also flow within the sea water and across the seafloor interface. The total electromagnetic field is sensed at a seafloor receiver location as the summation of the primary and secondary fields. The total field is recorded by one or several receivers (RXs) that are deployed before the TX tow is started. Similar to the apparatus used in seismic exploration, a towed streamer-based EM system is also possible and has been studied. However, in this thesis, the focus is on the conventional type of MCSEM method, in which seafloor receivers are deployed (Figure 2).

MCSEM data acquisition geometry can be divided into two end-member cases according to the relative geometry of the transmitter and a given receiver; either inline or broadside. In the inline case, the receiver is located along the path of the towed transmitter; in the broadside case, the receiver is located along a line perpendicular to the

transmitter alignment. There are many other receiver locations possible that yield a hybrid of the inline and broadside cases.

MCSEM modes can also be defined by the geometry of electric currents that are induced in the Earth (Chave, 2009). Transverse electric (TE) and transverse magnetic (TM) modes are possible. The TE mode is characterized by horizontal loops of electric current flowing in the subsurface. The TM mode is characterized by vertical loops. Separation into independent TE and TM modes is possible only in the case of a 1-D layered earth.

The TM mode, sometimes loosely called the "galvanic mode", is the more effective one to detect resistive zones. The normal component of the electric field exhibits a rapid change across an interface from a conductive medium to a resistive medium. This is because the total current $\mathbf{J}$ must be continuous across the interface of the two media. Hence, by Ohm's law $\mathbf{J} = \sigma\mathbf{E}$, the electrical conductivity σ is proportionately reduced, abruptly increasing the electric field $\mathbf{E}$. This feature is key to MCSEM detection of hydrocarbon reservoirs since hydrocarbons are much less conductive (more resistive) than seawater.

Whenever low-frequency electromagnetic fields are measured, as in MCSEM, it is important to consider the skin effect. An MCSEM transmitter injects low-frequency (0.1-10Hz) signals into the high electrical conductivity medium of seawater. Electromagnetic fields in the low-frequency regime decay exponentially with depth of penetration. The skin depth is

$$d_s \equiv \frac{500}{\sqrt{\sigma f}};$$

where σ is conductivity of the medium in $[^{S}/_{m}]$, and f is the frequency of transmitter in [Hz]. Thus, the skin depth d_s is expressed in [m]. Some other key features of MCSEM are shown in Table 1.

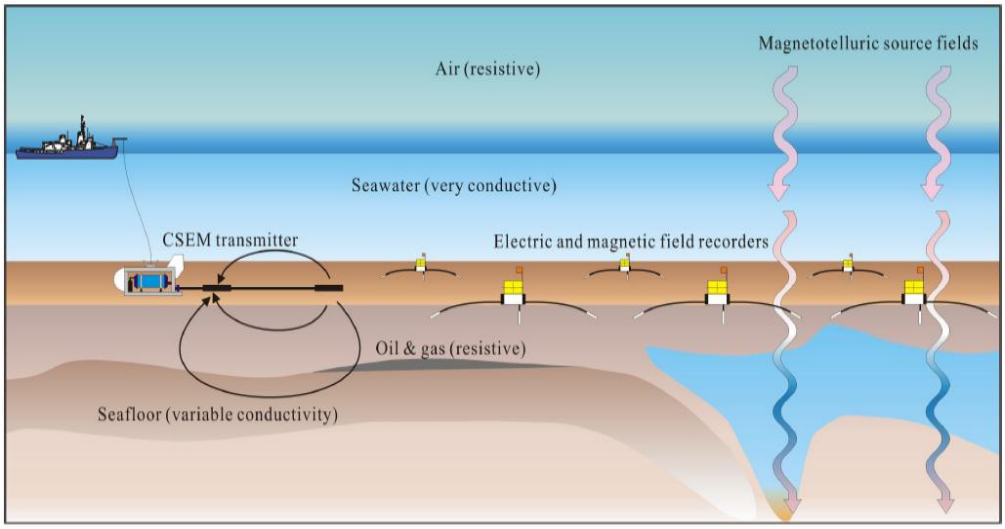

Figure 2. The conventional MCSEM acquisition setup with horizontal electric dipole source towed by a vessel and seafloor receivers (Constable and Srnka, 2007).[**]

[**] Reprinted with permission from "An introduction to marine controlled-source electromagnetic methods for hydrocarbon exploration." by Constable and Srnka, 2007, *Geophysics*, 72, No. 2, P. WA3-WA12, Copyright 2007 by SEG

Table 1. Key features of MCSEM

Band of Frequency	0.1~ 10 Hz
Source (TX)	Horizontal Electric dipole (HED) (500~1000A)
Receiver (RXs)	One or several array on the seafloor
Skin depth	Hundreds of m ~ several of km
Target	Subsurface materials with different resistivity
Measurement	E_x, E_y
Use	Exploration of Hydrocarbon reservoir, etc
Key factors	Apparent resistivity, phase, etc

2. THEORETICAL APPROACH

2.1 Previous studies

Many theoretical studies of the EM geophysical technique have been conducted. The problem of finding the electromagnetic fields due to various dipole sources (Sommerfeld 1964) is the classic reference for the case that the medium is a uniform isotropic halfspace. Related problems involving electrical and magnetic dipoles over a stratified isotropic medium were solved by Wait (1951, 1953). Solutions for various dipole sources over a stratified anisotropic medium were shown by Kong (1972). In addition, the problem of electric dipole excitation of an isotropic double half-space was solved in Everett (1990). In most previous theoretical works, as herein, the analytic solutions are formulated in terms of Sommerfeld's Hertz vector potential.

Bannister (1968) presented the theory for a frequency-domain, seafloor-to-seafloor dipole-dipole exploration system. Since then, calculations of the electromagnetic response to controlled-source systems have been extensively explored, including; the magnetic dipole-dipole configuration in the time domain (Cheesman *et al*. 1993), the electric dipole-dipole configuration in the time domain (Cairns *et al*. 1996), and the electric dipole-dipole configuration in the frequency domain (Cox *et al*. 1986). As a result of the previous studies, it has been determined that the frequency-domain technique, rather than the time-domain technique, is most suitable for deep (1~5km) hydrocarbon-reservoir exploration.

In MCSEM, it is conventional to locate the TX at the origin of a polar coordinate system (ρ, ϕ) and decompose the horizontal electric field at a remote RX location into its radial E and azimuthal E_{ϕ} components. However, when modeling the response of anisotropic structures, the decomposition of electric field into anisotropy strike-parallel, denoted ($\parallel$), and strike-perpendicular, denoted ($\perp$), is preferred (Yu and Edwards 1992). The conductivity of the anisotropic layer is similarly decomposed into its strike-parallel $\sigma_{\parallel}$ and strike-perpendicular $\sigma_{\perp}$ components.

2.2 MCSEM anisotropic modeling concept

In geophysical exploration, isotropic Earth forward modeling techniques have been developed and the appropriate measured data have been interpreted by inversion methods. Isotropic Earth models have a simpler structure than anisotropic models. However, most of the actual Earth exhibits anisotropic physical properties. Generally, anisotropy in Earth properties is complicated to understand and the non-intuitive responses make interpretation difficult. Herein I evaluate the controlled-source electromagnetic response in the frequency domain due to a horizontal electric dipole (HED) transmitter situated over a seafloor comprising a uniaxial vertically anisotropic layer overlying an isotropic basement.

Nominally, the uniaxial layer represents a thin-layered earth formation that has developed by sedimentation over geological time. Unlike an isotropic layer, a uniaxial anisotropic layer has different characteristics along different directions. The possible realizations of a uniaxial layer are shown in Figure 3. A vertical anisotropic Earth model exhibits conductivity tensor $\underline{\sigma} = diag(\sigma_{\parallel}, \sigma_{\parallel}, \sigma_{\perp})$. To model a thinly bedded formation,

as in Figure.3 (bottom right), the conductivity in the two horizontal (x, y) directions is kept the same, while its value is smaller in the z-direction ($\sigma_{\parallel} > \sigma_{\perp}$). Under these conditions, the charge carriers prefer move horizontally along the conductive sheets. Vertical charge carrier motion is restricted since the charges must migrate across the resistive sheets.

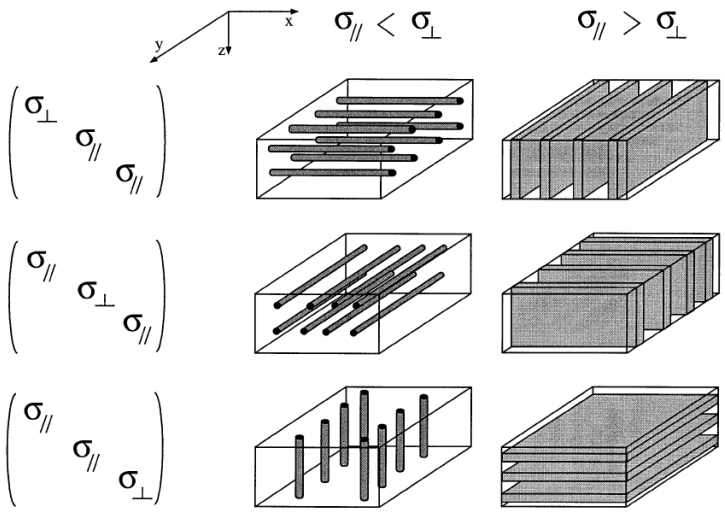

Figure 3. Physical realizations of a medium characterized by a uniaxial electrical conductivity tensor (Everett and S. Constable, 1999).[***]

The envisioned MCSEM forward modeling scenario in Cartesian geometry is shown in Figure 4. The horizontal electric field at the seafloor receiver sites is generated by an HED transmitter with moment P deployed over a seafloor consisting of an

[***] Reprinted with permission from "Electric dipole fields over an anisotropic seafloor: theory and application to the structure of 40 Ma Pacific Ocean lithosphere" by Everett, M.E. and Constable, S.C., 1999, 136, P 41-56, Copyright 1999 by *Geophysics Journal International.*

isotropic, seawater half space underlain by the two-layered structure consisting of a uniaxial overburden and an isotropic basement. The HED transmitter, which is directed at arbitrary angle Φ measured positive clockwise with respect to the Cartesian *y* direction, is located at height *h* above seafloor (*z*=0). Thus, the x-directed HED source is directed at $\Phi = 270$. Generally, the seawater conductivity is $\sigma_w = \sigma_0 = 3.2$ [S/m]. The upper Earth layer is uniaxial, which means its conductivity is described by tensor $\underline{\sigma} = diag(\sigma_{\parallel}, \sigma_{\parallel}, \sigma_{\perp})$ (Figure 3). This form is appropriate to describe the finely-bedded sediments of the uniaxial layer. The isotropic basement is of conductivity σ_3. Finally, the resistive disk (hydrocarbon reservoir) has been located below the uniaxial layer.

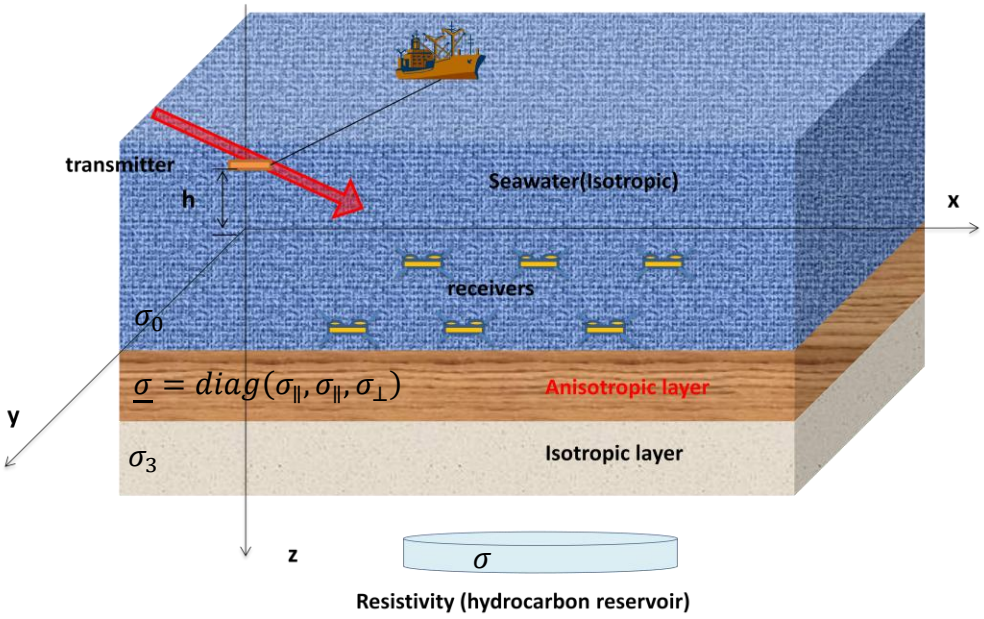

Figure 4. A marine controlled-source electromagnetic (CSEM) system deployed over a uniaxial seafloor overlying a resistive disk.

2.3 Analytic solution for a uniaxial model

The asymmetry of electrical conductivity due to the anisotropic medium precludes the use of Hankel transforms to develop analytic solutions to CSEM problems. However, it is possible (Yu and Edwards 1992; Everett and Constable 1999; Al-Garni and Everett 2003) in the case of a uniaxial medium with horizontal anisotropy to directly solve for the horizontal electric field components e_x, e_y in the 2-D Fourier wavenumber domain (p, q). The 2-D Fourier transform and its inverse are defined as

$$f(p,q) = \int_{-\infty}^{\infty}\int_{-\infty}^{\infty} F(x,y)exp(+ipx + iqy)dxdy; \tag{1}$$

$$F(x,y) = \frac{1}{4\pi^2}\int_{-\infty}^{\infty}\int_{-\infty}^{\infty} f(p,q)exp(-ipx - iqy)dpdq. \tag{2}$$

Once $e_x(p,q)$, $e_y(p,q)$ are found, double–sine and double–cosine transforms are applied to recover the electric field constituents E_x, E_y in the spatial (x, y) domain. Lower-case symbols represent EM field components in the double wavenumber domain while upper-case symbols denote spatial domain components. The frequency range is typically 0.1-10 Hz (Cox *et al*. 1986; Constable and Cox, 1996). The governing equations are the Maxwell's equations and the time-harmonic excitation form is $exp(+i\omega t)$. Ampere's and Faraday's laws in this frequency range are

$$\boldsymbol{\nabla} \times \boldsymbol{E} = -i\omega \boldsymbol{B} \tag{3}$$

$$\boldsymbol{\nabla} \times \boldsymbol{B} = \mu_0 \underline{\sigma} \boldsymbol{E} + \mu_0 \boldsymbol{J}_s \tag{4}$$

where ω is angular frequency, μ_0 is the magnetic permeability of free space, and $\boldsymbol{J}_s$ illustrates the electric current density of the source.

I am interested in determining the MCSEM response of a layered medium exhibiting vertical anisotropy. Using a similar approach to those of Yu and Edwards (1992) and Everett and Constable (1999) to solve equations (3) and (4), the following partial differential equation (PDE) is shown to be obeyed by the vertical component E_z of the electric field (Appendix A):

$$-\frac{\partial^2 E_z}{\partial x^2}-\frac{\partial^2 E_z}{\partial y^2}-\frac{\sigma_\perp}{\sigma_\parallel}\frac{\partial^2 E_z}{\partial z^2}+i\omega\mu_0\sigma_\perp E_z=0. \tag{5}$$

This PDE can be solved with a 2-D Fourier transform in the (*x*, *y*) directions. However, note that equation (5) is formulated in terms of the *z*-component of the electric field, since the uniaxial conductivity ($\sigma_\perp, \sigma_\parallel, \sigma_\parallel$) of a vertically anisotropic medium makes it difficult to solve directly for the horizontal electric field components.

To apply the fundamental boundary conditions of electromagnetics, the solution for the *z*-component of electric field E_z has to be converted into the *x*-, and *y*-components since it is E_x, E_y that are continuous at each interface. The second-order derivatives $\partial^2/\partial x^2$ and $\partial^2/\partial y^2$ in the spatial domain correspond to multiplications in the wavenumber by $-p^2$ and $-q^2$, since the partial derivatives and wavenumber are related by $\partial/\partial x = ip, \partial/\partial y = iq$.

In the (p, q) wavenumber domain, it is east to see find the ordinary differential equation (ODE) obeyed by the vertical electric field:

$$\frac{d^2 e_z}{dz}-u_2^2 e_z=0, \tag{6}$$

where $u_2 \equiv \sqrt{{\sigma_\parallel}/{\sigma_\perp}\,(p^2+q^2) + i\omega\mu_0\sigma_\parallel}$. A similar ODE can be induced for the across-strike vertical magnetic field:

$$\frac{d^2 b_z}{dz} - u_1^2 b_z = 0, \tag{7}$$

where $u_1 \equiv \sqrt{p^2+q^2+i\omega\mu_0\sigma_\perp}$. In the isotropic parts of the electrical conductivity structure, namely the seawater and isotropic basement, in each case the two conductivities $\sigma_\perp, \sigma_\parallel$ are converted to a single value, either σ_0 or σ_3, respectively. Thus, u_0 and u_3 are defined as $u_0 \equiv \sqrt{p^2+q^2+i\omega\mu_0\sigma_0}$, $u_3 \equiv \sqrt{p^2+q^2+i\omega\mu_0\sigma_3}$. The source term (HED) is located above the seafloor at height h. The symbols σ_0 and σ_w are used interchangeably.

The EM field components e_z^0, b_z^0 in medium 0, beneath the HED source but above the seafloor, have the form:

$$e_z^0(p,q) = \Gamma_1\, exp(-u_0 z) + A\, exp(u_0 z); \tag{8}$$

$$b_z^0(p,q) = \Gamma_2\, exp(-u_0 z) + B\, exp(u_0 z). \tag{9}$$

The coefficients Γ_1 , Γ_2 represent the downward diffusion of the primary EM field from the transmitter to the seafloor. These source terms are derived using the Hertz vector (Appendix B). The *A* and *B* coefficients are upward diffusing fields due to a 'reflection' from the seafloor. The coefficients are determined by application of boundary conditions. In the anisotropic medium 1, the vertical EM field components are

$$e_z^1(p,q) = C\, exp(-u_2 z) + D\, exp(u_2 z); \tag{10}$$

$$b_z^1(p,q) = E\, exp(-u_1 z) + F\, exp(u_1 z). \tag{11}$$

The coefficients *C*, *E* represent downward diffusion due to 'transmission' of the EM fields into the seafloor. The coefficients *D*, *F* are upward diffusing fields due to 'reflection' from the isotropic basement which is located beneath the anisotropic medium.

In the isotropic basement, medium 2,

$$e_z^2(p,q) = G\, exp(-u_3 z)\,; \tag{12}$$

$$b_z^2(p,q) = H\, exp(-u_3 z). \tag{13}$$

The coefficients *G*, *H* represent the downward diffusion due to 'transmission' of the EM fields, and there is no 'reflection' since this is the basal layer, or terminating lower half-space.

In accordance with fundamental boundary conditions of electromagnetics, the tangential EM field components (e_x, b_x, e_y, b_y) must be continuous at the each interface. The vertical e_z, b_z components are given by equations (8-13); however, the tangential components (e_x, b_x, e_y, b_y) are not yet determined. They are found by converting Ampere's and Faraday's laws:

$$\boldsymbol{\nabla} \times \boldsymbol{e} = -i\omega \boldsymbol{b}; \tag{14}$$

$$\boldsymbol{\nabla} \times \boldsymbol{b} = \mu \underline{\sigma} \boldsymbol{e}. \tag{15}$$

into wavenumber domain, and using the continuity equation of the electric field, and the divergence free condition of the magnetic field. The final forms of the tangential components $\left(e_x, b_x, e_y, b_y\right)$ expressed in terms of the vertical components (e_z, b_z) are (Appendix C);

$$e_x = \frac{1}{\sigma_{\|}(p^2+q^2)}(i\partial_z\sigma_{\perp}pe_z + w\sigma_{\|}qb_z); \tag{16}$$

$$e_y = \frac{1}{\sigma_{\|}(p^2+q^2)}(i\partial_z\sigma_{\perp}qe_z - w\sigma_{\|}pb_z); \tag{17}$$

$$b_x = \frac{i}{p^2+q^2}(p\partial_z b_z + \mu\sigma_{\perp}qe_z); \tag{18}$$

$$b_y = \frac{i}{p^2+q^2}(q\partial_z b_z - \mu\sigma_{\perp}pe_z). \tag{19}$$

The boundary conditions on the tangential components of electric and magnetic fields at each interface yield 8 linear complex equations for the 8 unknown coefficients *A*-*H*. Thus, a 8×8 complex linear system must be solved. The terms including Γ_1, Γ_2 are known and are moved to the right hand side (Appendix D). The complex 8×8 linear system is expanded into a 16×16 real system of equations and this matrix is solved by standard numerical methods.

After numerical calculation of the *A*-*H* coefficients, each coefficient can be substituted into the expressions (16-19) for each layer, such that the (p, q)-domain electric fields within each medium are expressed as

$$e_x^0(p,q) = \frac{-iu_0p\Gamma_1 + wq\Gamma_2}{(p^2+q^2)}exp(-u_0z) + \frac{iu_0pA + wqB}{(p^2+q^2)}exp(u_0z); \tag{20}$$

$$e_x^1(p,q) = \frac{-iu_2\sigma_{\perp}p\ C}{\sigma_{\|}(p^2+q^2)}exp(-u_2z) + \frac{w\sigma_{\|}qE}{\sigma_{\|}(p^2+q^2)}exp(-u_1z) + \frac{iu_2\sigma_{\perp}p\ D}{\sigma_{\|}(p^2+q^2)}exp(u_2z) + \frac{wq\ F}{(p^2+q^2)}exp(u_1z); \tag{21}$$

$$e_x^2(p,q) = \frac{i(-u_3)pG + wqH}{(p^2+q^2)}exp(-u_3z)\,; \tag{22}$$

$$e_y^0 = \frac{-iu_0 q\Gamma_1 - wp\Gamma_2}{(p^2+q^2)} exp(-u_0 z) + \frac{iu_0 qA - wpB}{(p^2+q^2)} exp(u_0 z); \quad (23)$$

$$e_y^1 = \frac{-iu_2 qC}{(p^2+q^2)} exp(-u_2 z) + \frac{-w\sigma_{\|} pE}{\sigma_{\perp}(p^2+q^2)} exp(-u_1 z)$$

$$+ \frac{-w\sigma_{\|} pF}{\sigma_{\perp}(p^2+q^2)} exp(u_1 z) + \frac{iu_2 q}{(p^2+q^2)} Dexp(u_2 z); \quad (24)$$

$$e_y^2 = \frac{-iu_3 qG - wpH}{(p^2+q^2)} exp(-u_3 z). \quad (25)$$

Likewise, the (p, q)-domain magnetic fields within each medium are

$$b_x^0(p,q) = \frac{ip(-u_0)\Gamma_2 + \mu\sigma_w q\Gamma_1}{p^2+q^2} exp(-u_0 z) + \frac{ipu_0\, B + \mu\sigma_w q\, A}{p^2+q^2} exp(u_0 z); \quad (26)$$

$$b_x^1 = \frac{-ipu_1 E}{p^2+q^2} exp(-u_1 z) + \frac{ipu_1 F}{p^2+q^2} exp(u_1 z)$$

$$+ \frac{i\mu\sigma_{\perp} qC}{p^2+q^2} exp(-u_2 z) + \frac{i\mu\sigma_{\perp} qCD}{p^2+q^2} exp(u_2 z); \quad (27)$$

$$b_x^2 = \frac{i(-pu_3 H + \mu\sigma_3 qG)}{p^2+q^2} exp(-u_3 z); \quad (28)$$

$$b_y^0 = \frac{-i(qu_0\Gamma_2 + \mu\sigma_w p\Gamma_1)}{p^2+q^2} exp(-u_0 z) + \frac{i(qu_0 B - \mu\sigma_w pA)}{p^2+q^2} exp(u_0 z); \quad (29)$$

$$b_y^1(p,q) = \frac{iq(-u_1)E}{p^2+q^2} exp(-u_1 z) - \frac{i\mu\sigma_{\perp} pC}{p^2+q^2} exp(-u_2 z)$$

$$+ \frac{iqu_1 F}{p^2+q^2} exp(u_1 z) - \frac{i\mu\sigma_{\perp} p\, D}{p^2+q^2} exp(u_2 z); \quad (30)$$

$$b_y^2(p,q) = \frac{-iqu_3 H - \mu\sigma_3 pG}{p^2+q^2} exp(-u_3 z). \quad (31)$$

Generally, the MCSEM technique measures the spatial-domain E_x, E_y components at seafloor receiver locations. The 2-D inverse Fourier transforms retrieve

the spatial variations of the horizontal electric field, as described in equation (2). The receivers are located on the seafloor, therefore, the 2-D inverse Fourier transform is only required for e_x^0, e_y^0. The spatial-domain E_x, E_y components are found using

$$E_x(x,y) = \frac{1}{4\pi^2}\int_{-\infty}^{\infty}\int_{-\infty}^{\infty} e_x^0(p,q)exp(-ipx - iqy)dpdq; \tag{32}$$

$$E_y(x,y) = \frac{1}{4\pi^2}\int_{-\infty}^{\infty}\int_{-\infty}^{\infty} e_y^0(p,q)exp(-ipx - iqy)dpdq. \tag{33}$$

These calculations are performed by numerical methods. The solutions (32-33) are the predicted MCSEM responses on a seafloor overlying a uniaxial layer with isotropic basement.

3. NUMERICAL APPROACH

3.1 Previous studies and forward models

Transient MCSEM numerical modeling was developed by Everett and Edwards (1992). They presented 2.5-D responses (3-D source and 2-D earth model) using a finite-element method. Unsworth *et al*. (1993) suggested a similar 2.5-D finite-element numerical solution in the frequency domain. Sinha (1999) showed with 1-D modeling that higher resistivity layers within the subsurface are best detected by an inline TX-RX configuration.

The 3-D forward modeling code SEATEM, based on a finite element algorithm, was developed by Badea *et al.* (2001) initially to analyze electromagnetic well logging responses. The SEATEM code has been validated for 1-D, 2-D and 3-D structures and has local refinement capabilities for building fine-scale tetrahedral finite-element meshes. A locally-refined mesh allows a user to easily model thin resistive layers or zones in the subsurface.

King (2004) used a version of the SEATEM code modified for MCSEM to develop frequency-domain forward modeling of various resistive disks and their responses. Dickins (2007) used SEATEM to investigate MCSEM survey designs for imaging hydrocarbon-saturated zones, in particular to understand the masking effect of an overlying gas hydrate layer.

As a result of this and other previous experience, three types of MCSEM SEATEM models have been developed: a uniform double halfspace (Type I) composed

of an upper seawater and a lower seafloor layer; a buried disk (Type II) regarded as a hydrocarbon reservoir; a buried disk with a vertical cylinder (Type III) regarded as a steel pipe. These models are illustrated in Figure 5.

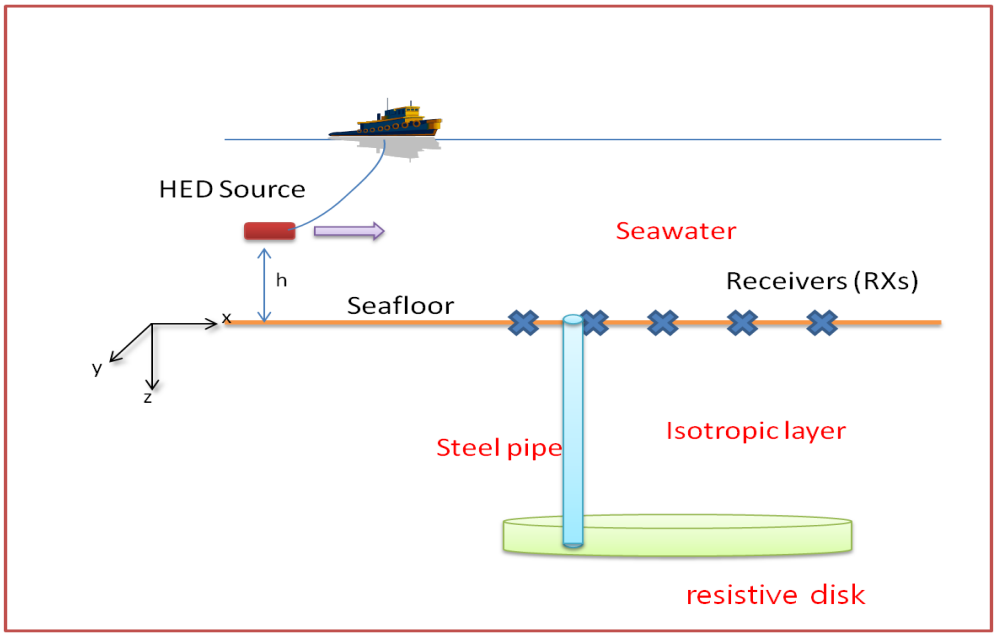

Figure 5. Three different types of SEATEM models.

3.2 Methodology

The SEATEM algorithm has been used to calculate 3-D MCSEM responses in isotropic conductive media. This research uses the SEATEM algorithm to understand the effect of an anisotropic layer on the MCSEM response. As demonstrated by the previous research, the SEATEM code can be used to developing forward Earth models of interest to MCSEM practitioners. The SEATEM algorithm was first validated against a 1-D shallow-water MCSEM solutions for an *x*-directed HED and since then has been used to calculate the responses of various types of 3-D Earth models containing thin resistive

zones. The SEATEM code is composed of three parts: a header file (`cylmesh.h`); input files (`seatem1.in, seatem2.in, seatem3.in, lra.in`); and calculation and output files (`seatem1.f, seatem2.f, and seatem3.f`).

The SEATEM mesh structure is illustrated in Figure 6. The mesh, composed of tetrahedra, is generated in the `seatem1.f` module. The size of the mesh is specified in the header file `cylmesh.h`. The local refinement capability is helpful to accurately model the response at very small TX-RX offsets. The local refinement regions are specified in the file `lra.in`. After generating the mesh, the primary electric fields based on a Hankel transform solution are calculated. The method to solve the Hankel transform is selected in the input file `seatem2.in`. There are two different numerical approaches to performing the Hankel transform, the Chave (1983) and Gutasarma-Singh (1997) methods. The calculation of the primary and secondary electric fields is performed in `seatem2.f`. After solving for the primary and the secondary electric fields, the total electric field is calculated and some post-processing is done in `seatem3.f`. The logical structure of SEATEM is shown in Figure 7.

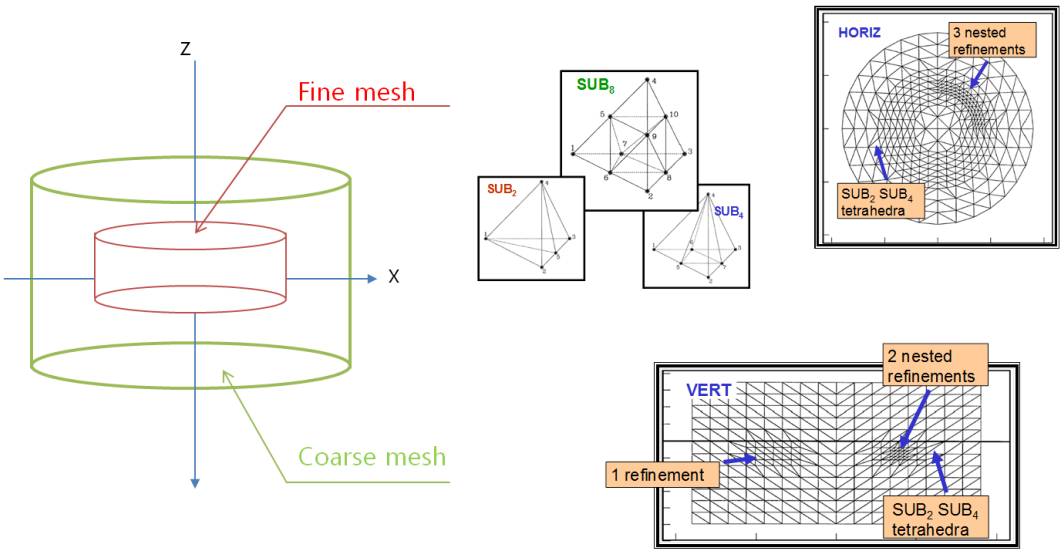

Figure 6. The tetrahedron mesh structure of CSEM and its refinement to increase resolutions (Everett 2006)

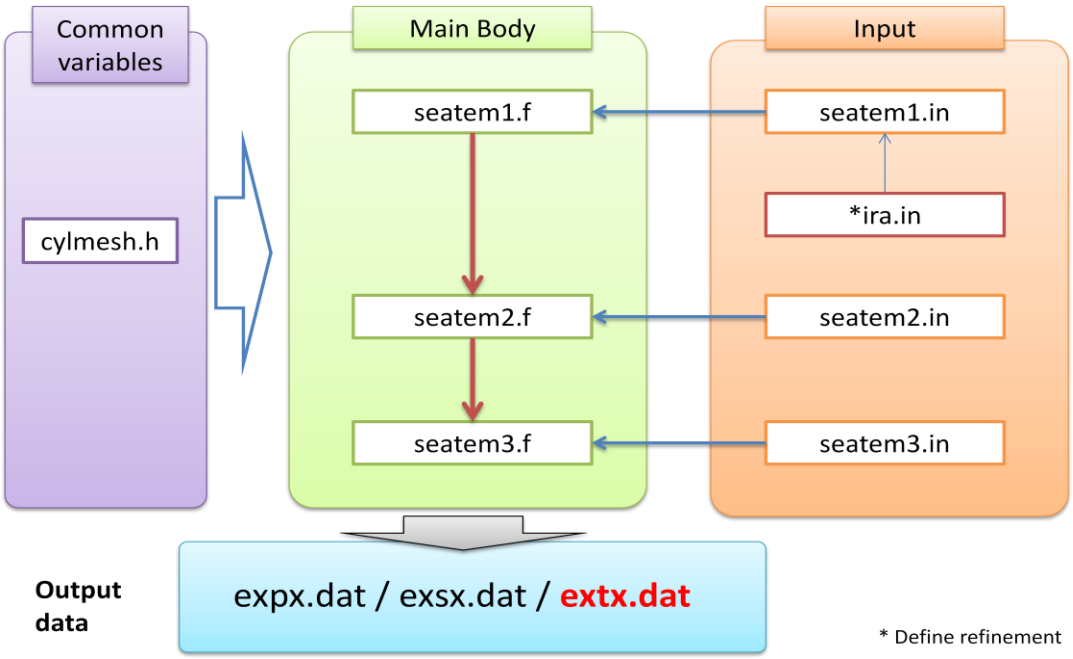

Figure 7. A logical structure of SEATEM codes.

To generate a uniaxial anisotropic Earth model from an original isotropic model, the single uniform conductivity parameter must be split into three anisotropic conductivities, one for each of the *x*, *y* and *z* directions. In this research, the strike-parallel *x*, *y* components (σ_x, σ_y) have the same value ($\sigma_\parallel$) which is larger than the strike-perpendicular *z* component ($\sigma_z = \sigma_\perp$). The condition ($\sigma_\parallel > \sigma_\perp$) appropriate for modeling a thin-bedded formation was discussed in a previous section of this thesis. I have made the necessary modifications in the SEATEM code to split the one variable into three variables.

After expanding one parameter $\sigma_{uniform}$ into three parameters σ_x, σ_y and σ_z within the SEATEM code, a procedure is required to validate the modification. This is done by comparison with previous modeling results. Thus, the new anisotropic model, named Type IV, is tested by finding the MCSEM response of an isotropic model using the newly-modified SEATEM code. This is done by setting $\sigma_x = \sigma_y = \sigma_z$. The anisotropic response is expected in this case to reduce to the equivalent isotropic response. The isotropic EX-EX response is shown by King (2004). In agreement with this previous result, the total electric field computed herein using the modified SEATEM code indeed attenuates in the expected manner with TX-RX offset, as demonstrated in Figure 8.

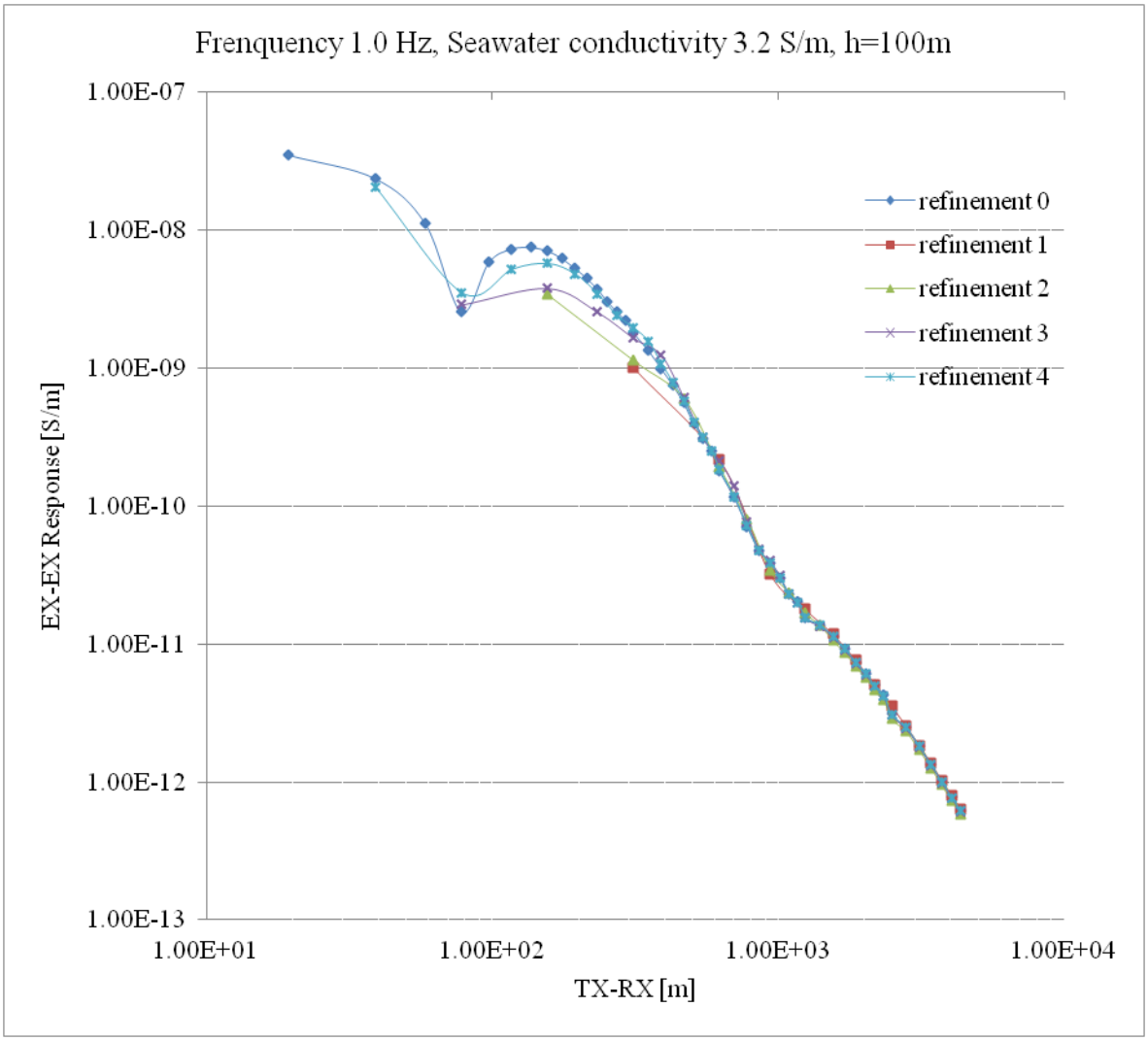

Figure 8. The isotropic EX-EX responses for an isotropic halfspace results, computed to validate the anisotropy modification of the SEATEM code.

3.3 Results and discussion

The anisotropic halfspace

The previous research of King (2004) and Dickins (2007) demonstrated MCSEM forward modeling in isotropic media. The uniform double halfspace model (Type I) is characterized by isotropic seawater overlying an isotropic basement, and its response is illustrated in Figure 8. The isotropic response is useful as a baseline to compare the influence of an anisotropic layer, as in the Type IV model. The assumed uniaxial conductivity has diagonal conductivity tensor $\underline{\sigma} = (\sigma_{\parallel}, \sigma_{\parallel}, \sigma_{\perp})$ appropriate for thinly-bedded sediments. Parameters for various modeling scenarios are presented in Table 2.

EX-EX responses for different uniaxial models of Type IV are shown in Figures 9 and 10. Comparing to the isotropic response (blue line), the anisotropic responses show a pronounced anomaly at TX-RX offset ~1 km. The anomaly is due to reflection of the primary field at the anisotropic layer. At TX-RX offsets beyond the anomalous range, the EX-EX response of the isotropic model is recovered. There is also a significant dependence on the value of the *z*-direction conductivity, $\sigma_{\perp}$.

In Figure 11, it can be seen that the total EXEX responses depend on the relative values of the conductivity in the strike-parallel and strike-perpendicular directions. The case $(\sigma_{\parallel} = 0.1, \sigma_{\perp} = 0.01)$ shows the most marked anomaly at offset ~1 km. The case $(\sigma_{\parallel} = 0.01, \sigma_{\perp} = 0.001)$ shows a similar effect. Use of the local mesh refinement technique available in the SEATEM code generates the higher-resolution EXEX responses shown in Figure 12. The mesh refinement is carried out in the immediate vicinity of the transmitter. The EXEX respones diminish with TX-RX offset, just as

expected, although the anomaly at offset ~1 km shows considerable oscillation, as marked by the red circle in the figure.

There are two possible explanations for the oscillatory anomalous response, it could be caused either by the natural response of an anisotropic earth or by numerical modeling errors. A careful comparison should be made between the analytic solution derived earlier in this thesis and numerical solutions of the modified version of SEATEM. This work must be done in the future since it exceeds the scope of this thesis.

Table 2. Example parameters of anisotropic and isotropic models**.**

model	**Isotropic**	**Anisotropic**	**Anisotropic**	**isotropic**	**Anisotropic**	**Anisotropic**
refinement	0-4	0-4	0-4	0-4	0-4	0-4
σ_0 (σ_w)	3.2	3.2	3.2	3.2	3.2	3.2
$\sigma_\parallel$ (x-dir)	0.1	0.1	0.1	0.01	0.01	0.01
$\sigma_\parallel$ (y-dir)	0.1	0.1	0.1	0.01	0.01	0.01
$\sigma_\perp$ (z-dir)	0.1	0.01	0.001	0.01	0.001	0.0001

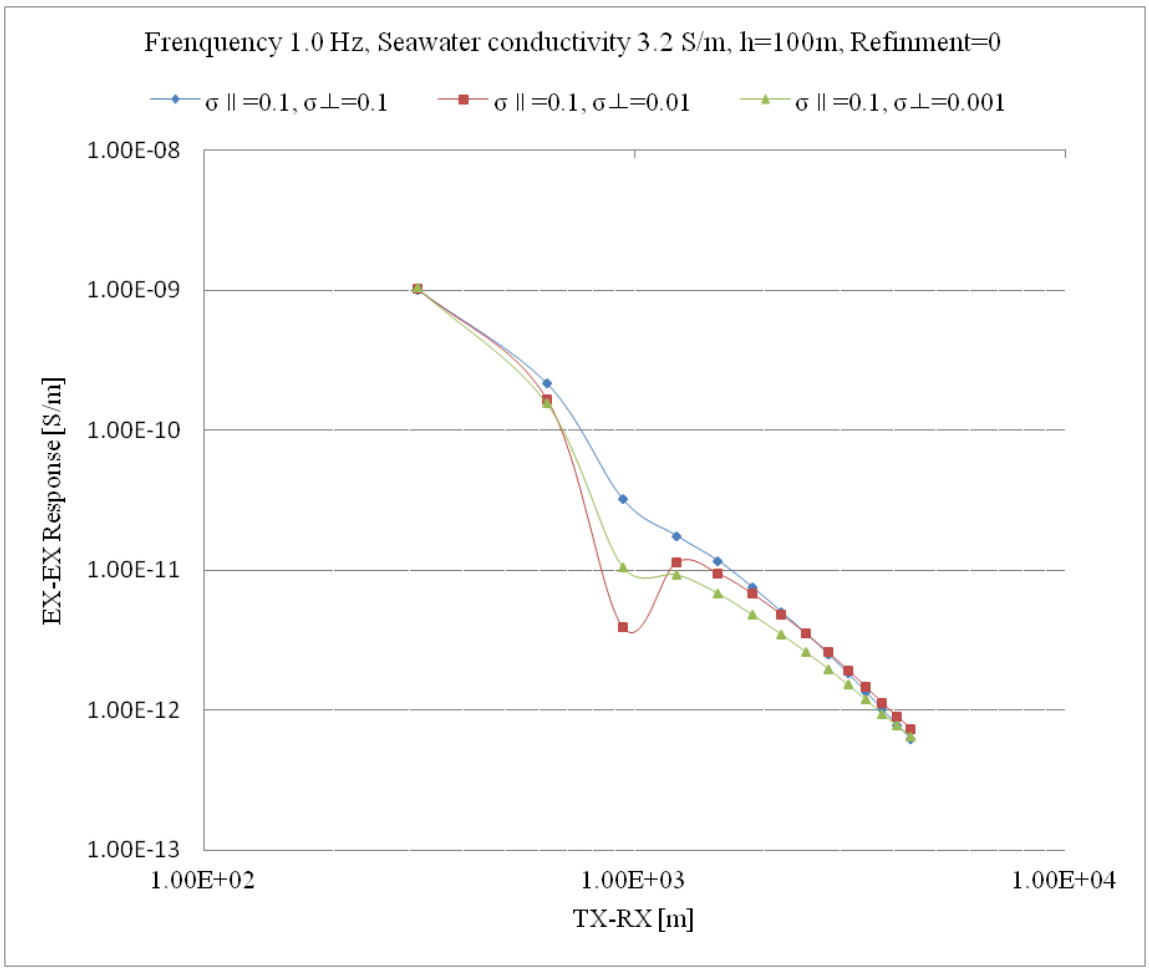

Figure 9. EX-EX responses for different values of the z-conductivity, $\boldsymbol{\sigma}_{\perp}$ with fixed horizontal conductivity $\boldsymbol{\sigma}_{\parallel}$ =0.1S/m.

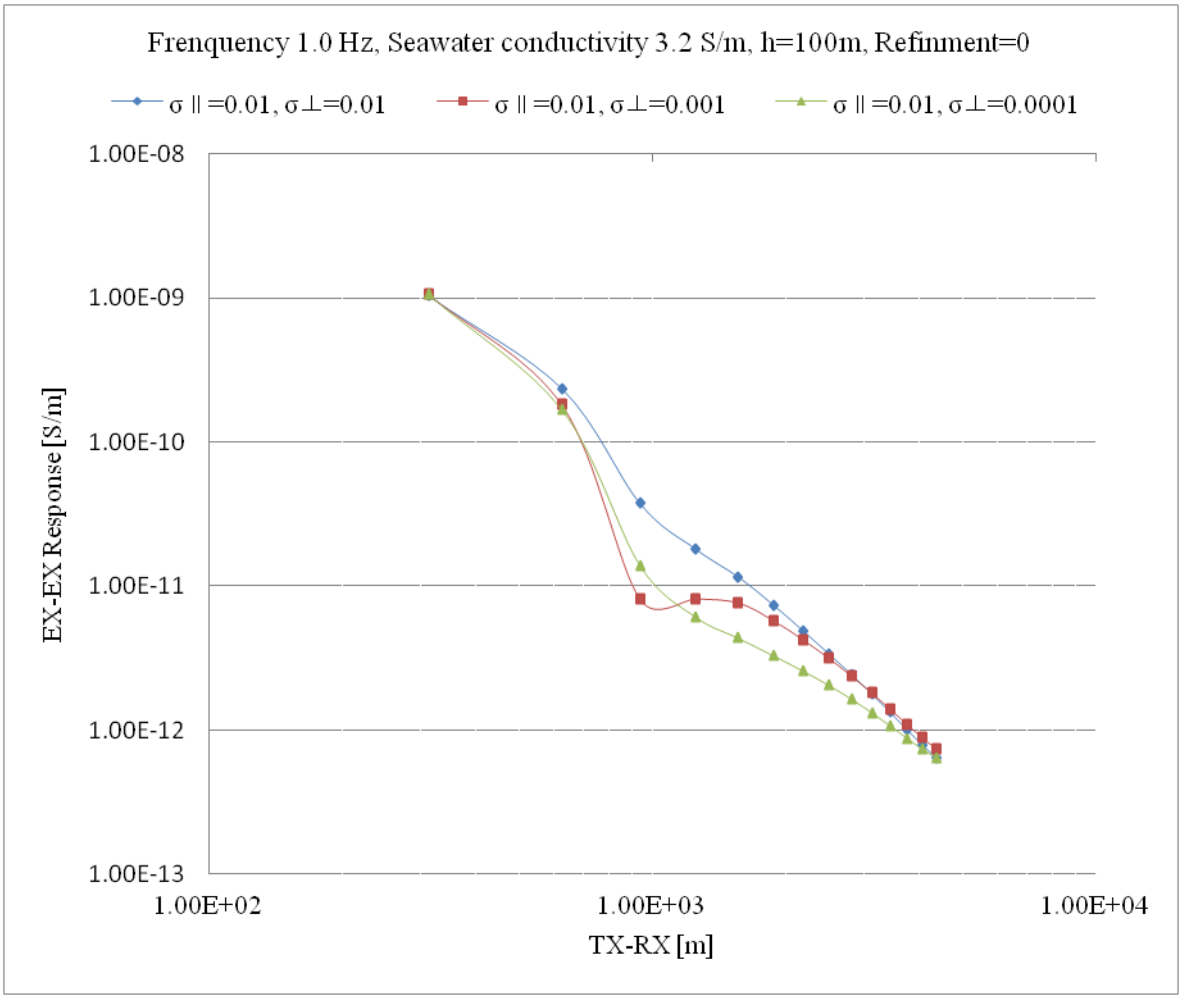

Figure 10. EX-EX responses for different values of the z-conductivity, $\boldsymbol{\sigma}_{\perp}$ with fixed horizontal conductivity $\boldsymbol{\sigma}_{\parallel}$ =0.01 S/m.

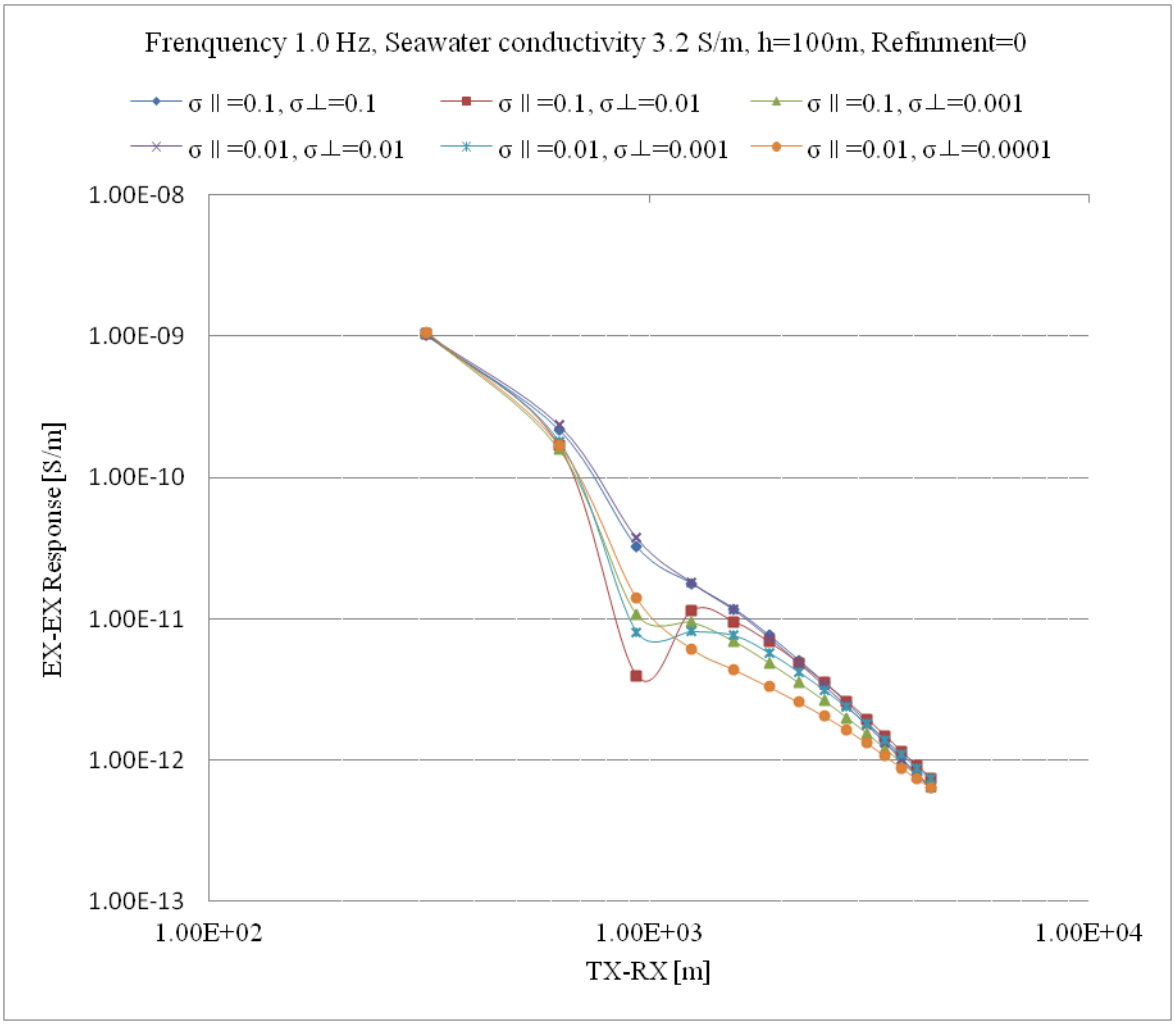

Figure 11. The responses of the previous two figures placed on a single plot.

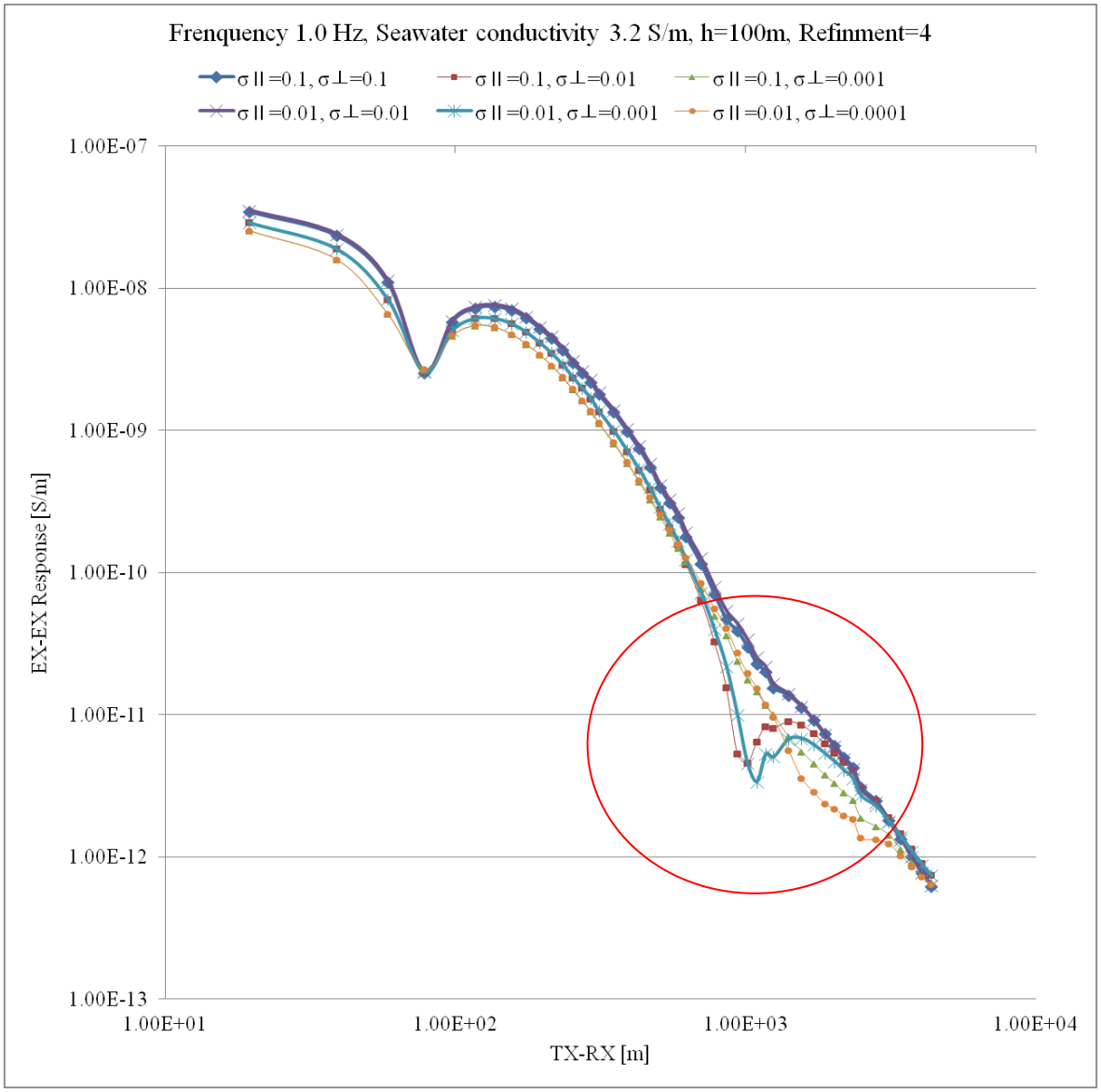

Figure 12. The responses shown in the previous figure, with mesh refinement.

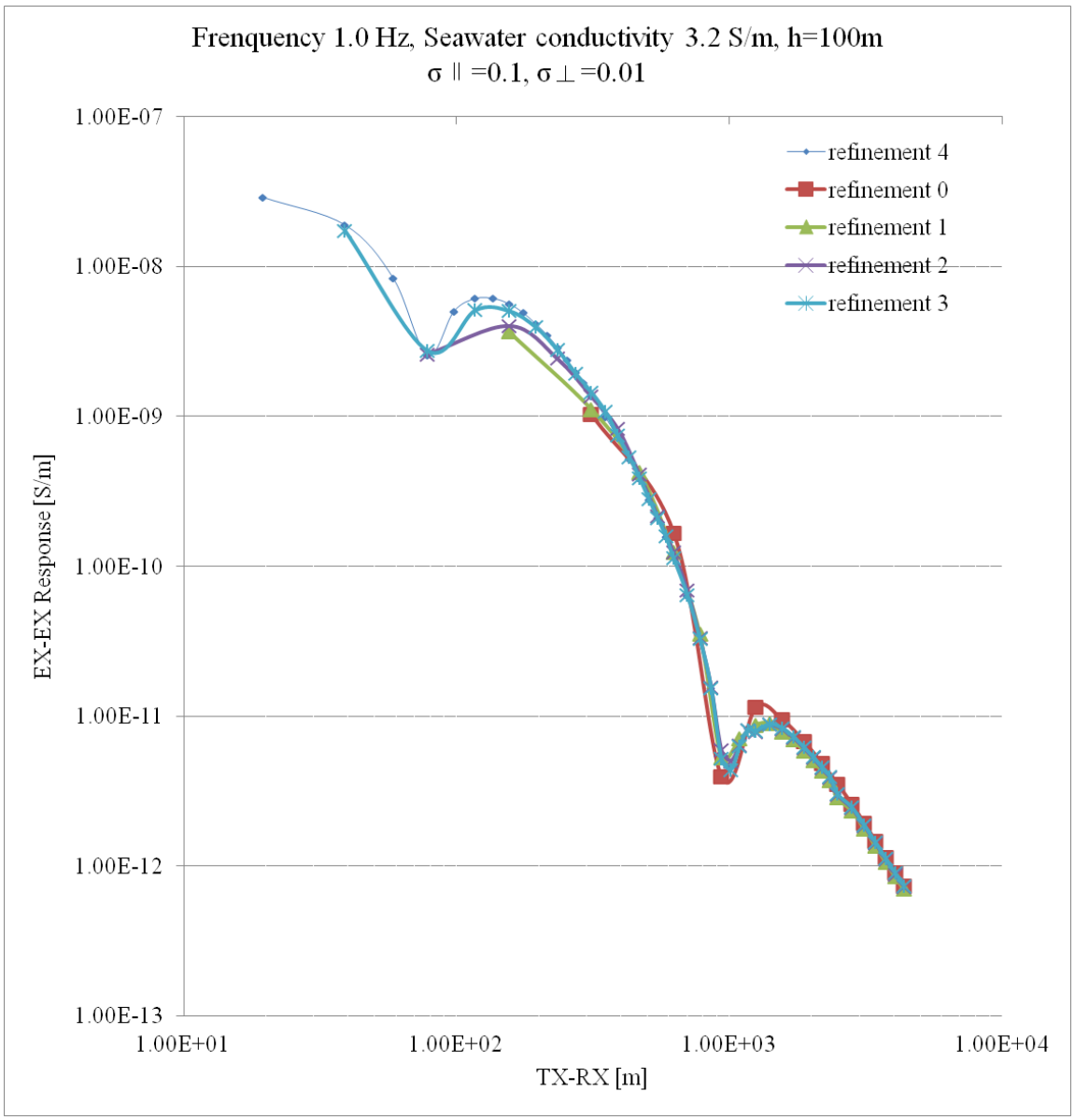

Figure 13. EX-EX responses of uniaxial model with different refinements

Buried disk under anisotropic layer

In the previous section, it is found that the uniaxial anisotropic model (Type IV) response contains an anomaly at TX-RX offset ~1 km. However, the explanation of the anomaly has not yet been confirmed by comparing the analytic solution with the output of the modified SEATEM code. Similar anomalies are also expected in the response of the buried disk (model Type V) beneath the anisotropic layer but this modeling has not yet been performed.

4. SUMMARY AND CONCLUSION

The MCSEM technique is a fast growing technology in exploration geophysics for offshore hydrocarbon reservoir characterization. The early period of MCSEM forward modeling presumed the Earth to be an isotropic conductive medium and calculations of MCSEM responses were made using FEM methods. An anisotropic Earth model is more realistic, but it can be difficult to interpret its response. The proper understanding of anisotropic Earth responses is essential however for making the best use of the MCSEM method in hydrocarbon exploration. Thus, a goal of this research is to understand the MCSEM response of a uniaxial earth model. This is best accomplished using both analytic solutions and numerical modeling. My research uses the modeling scenarios indicated in Figure 4.

Firstly, I found the analytical solution for a uniaxial Earth model composed of isotropic layers and an anisotropic layer, which has uniaxial components $(\sigma_{\parallel}, \sigma_{\parallel}, \sigma_{\perp})$ in Cartesian coordinates. The solution of diffusion equations in MCSEM model is required to be in the spatial (x, y) domain, but first it has to be converted to the double wavenumber (p, q) domain using a 2-D Fourier transform. The z-component of the conductivity $(\sigma_{\perp})$ of an anisotropic layer determines how the partial differential equation (PDE) is reduced to an ordinary differential equation (ODE). For a two-layer Earth beneath a uniform seafloor, there are eight unknown coefficients (A-H) and two source terms (Γ_1, Γ_2). The latter are found using the Hertz vector approach and expressed in terms of a Hankel transform. The fundamental boundary conditions of electromagnetics

require the tangential EM field components (e_x, b_x, e_y, b_y) to be continuous at each interface. Once these are applied, a 8×8 complex system of equations is found. This linear system is solved by a standard numerical method. Having acquiring the all coefficients, the spatial-domain solution E_x, E_y are obtained by an inverse 2-D Fourier transform, in particular, due to symmetry I can use double–sine and double–cosine transforms.

A modified SEATEM code is used for understanding the effect of an anisotropic layer and its responses. In the numerical modeling, a resistive disk is located below the anisotropic layer and its response found using the finite element method implemented in the SEATEM code. The model parameters for the anisotropic model have been updated from the previously-considered isotropic conductivity model (Type I). A single conductivity parameter has been split into three anisotropic conductivities. The anisotropic modeling codes are verified by comparison with an isotropic model response.

Numerical EX-EX responses for uniaxial models are comparing to the isotropic electric responses. The anisotropic response show significant anomalies at TX-RX offset ~1 km. The anisotropy EX-EX response also depends on the values of the strike-parallel and strike-perpendicular conductivities.

If the verification procedures, i.e. comparing the results of analytic solutions and modified SEATEM codes, continue to be successful, then the modified SEATEM code can be used widely in practical applications for hydrocarbon reservoir characterization. The modified code admits a different conductivity in each of the three Cartesian directions. This thesis considered only the horizontally bedded uniaxial anisotropic

model. Another uniaxial conductivity, a vertically thin bedded formation (Figure 3, right-top and right-middle), can be examined by using a diagonal tensor of the form $\underline{\sigma} = (\sigma_{\parallel}, \sigma_{\perp}, \sigma_{\parallel})$ or $\underline{\sigma} = (\sigma_{\perp}, \sigma_{\parallel}, \sigma_{\parallel})$. These types of models are suitable in active volcanic margin settings.

REFERENCES

Al-Garni, M. and Everett, M.E., 2003, The paradox of anisotropy in electromagnetic loop-loop responses over a uniaxial halfspace, *Geophysics*, 68, P.892-899

Badea, E.A., Everett, M.E., Newman, G.A. and Biro, O., 2001. Finite-element analysis of controlled-source electromagnetic induction using Coulomb-gauged potentials, *Geophysics*, 66, P.786-799.

Chave, A.D., 1983, Numerical integration of related Hankel transforms by quadrature and ontinued fraction expansion, *Geophysics*, 48, No. 12, P.1671-1686

Chave, A.D. and Cox, C.S., 1982, Controlled electromagnetic sources for measuring electrical conductivity beneath the oceans. 1. Forward problem and model study, *Journal of Geophysical Research*, 87, P.5327-5338.

Chave, A.D., Constable, S.C. and Edwards, R. N., 1991, Electrical exploration methods in applied Geophysics, *Society of Exploration Geophysicists*, 2, P.931-966.

Constable, S.C., Orange, A.S., Hoversten, G.M. and Morrison, H.F., 1998. Marine magnetotellurics for petroleum exploration Part I: A sea-floor equipment system, *Geophysics*, 63, No. 3, P.816-825.

Constable, S.C. and Cox, C.S., 1996. Marine controlled-source electromagnetic sounding 2. The PEGASUS experiment, *Journal of Geophysical Research*, 101, P.5519-5530.

Constable. S.C., 2010, Ten years of marine CSEM for hydrocarbon exploration, *Geophysics*, 75, No. 5, P.75A67-75A81

Constable, S.C. and Srnka L., 2007, An introduction to marine controlled-source electromagnetic methods for hydrocarbon exploration. *Geophysics*, 72, No. 2, P. WA3-WA12,

Cox, C.S., Constable, S.C., Chave, A.D. and Webb, S.C., 1986. Controlled-source electromagnetic sounding of the oceanic lithosphere, *Nature*, 320, No. 6057, P.52-54. 6 March

Dickins, D., 2007, Controlled-source electromagnetic modeling of the masking effect of marine gas hydrate on a deeper hydrocarbon reservoir, Texas A&M University, August

Ellingsrud, S., Eidesmo, T., Johansen, S., Sinha, M.C., Macgregor, L. M. and Constable, S. C., 2002, Remote sensing of hydrocarbon layers by seabed logging(SBL): Results from a cruise offshore Angola, *The Leading Edge*, 21, P.972-982.

Evans, R.L., Constable, S.C., Sinha, M.C., Cox, C.S. and Unsworth, M.J., 1991. Upper crustal resistivity structure of the East Pacific Rise near 13° N, *Geophysical Research Letters*, 18, P.1917-1920.

Evans, R.L., Sinha, M.C., Constable, S.C. and Unsworth, M.J, 1994. On the electrical nature of the axial melt zone at 13° N on the East Pacific Rise, *Journal of Geophysical Research*, 99, P.577-588.

Everett, M.E., 2012, Marine controlled-source electromagnetics for offshore hydrocarbon exploration, *Undergraduate Seminar*, Texas A&M University, October 30th

Everett, M.E. and Meju, M. A., 2005, Near-Surface Controlled-Source Electromagnetic Induction: Background and Recent Advances, 6.1. Introduction, *Hydrogeophysics*, Springer, P.157-158

Everett, M.E., 2006, Finite element analysis of shallow-water marine controlled-source electromagnetic signals for hydrocarbon exploration, *Marelec-2006: Marine Establishment*, Amsterdam, Netherlands, 19th~21st April

Everett, M.E. and Edwards, R.N., 1992. Transient marine electromagnetics: the 2.5-D forward problem, *Geophysics Journal International*, 113, P.545-561

Everett, M.E. and Constable, S.C., 1999, Electric dipole fields over an anisotropic seafloor:theory and application to the structure of 40 Ma Pacific Ocean lithosphere, *Geophysics Journal International,* 136, P 41-56

Guptasarma, D. and Singh, B., 1997, New digital linear filters for Hankel J0 and J1 transforms, *Geophysical Prospecting*, 45, No. 5, P.745-762

Hesthammer, J., Fanavoll, S., Stefatos, A., Danielsen, J.E. and Boulaenko, M., 2010, CSEM performance in light of well results; *The Leading Edge*, 29, No. 1, P.258-264

Jeon, Jaeho. 2008, CSEM(Controlled-source Electromagnetic) - A new tool for offshore exploration, KNOC, Geophysics, *E&P Technology Institute*, No. 672

Kong, J. A., 1972, Electromagnetic fields due to dipole antennas over stratified anisotropic media. *Geophysics*, 37, No 6, P. 985-996

King, J. D., 2004, Using a 3D finite element forward modeling code to analyze resistive structures with controlled-source electromagnetics in a marine environment, Texas A&M University, December

Kaufman, A. A. and Keller, G. V., 1983, Frequency and transient soundings, Elsvier Science Pub. Co. New York, N.Y..

Macgregor, L. M., Constable, S. C. and Sinha, M. C., 1998, The Remesses experiment-Ⅲ: Controlled source electromagnetic sounding of the Reyjanes Ridge at 57°45', *Journal of Geophysical Research*, 135, P.773-789.

Macgregor, L. M., Constable, S. C. and Sinha, M. C., 2001, Electrical resistivity structures of the Valu Fa Ridge, Lau basin, from marine controlled source electromagnetic sounding, *Geophysics Journal International*, 146, P.217-236.

Sommerfeld, A., 1964, Partial Differential Equations in Physics: Lectures on theoretical Physics, VI, Translated by E.G. Straus, *Academic Press*, P.335

Void, I.E., Rotevatn, A. and Hesthammer, J., 2012, The effect of hydrocarbon saturation on resistivity distribution and CSEM response, *Marine and Petroleum Geology*, 38, No. 1, P.117-127

Yu, L. and Edwards, R.N., 1992, The detection of lateral anisotropy of the ocean floor by electromagnetic methods, *Geophysics Journal International,*108, P.443-441

APPENDIX A

In this part, the ODE equation (6) from PDE equation (5) is shown. This result is derived from equations (3) and (4), and source-free regions($\boldsymbol{J}_s = 0$). Multiplying gradient $\boldsymbol{\nabla}$ to (3), and substitute $\boldsymbol{\nabla} \times \boldsymbol{B} = \mu_0 \underline{\sigma} \boldsymbol{E}$ in the equation (3), then the result of vector diffusion equation is

$$\boldsymbol{\nabla} \times \boldsymbol{\nabla} \times \boldsymbol{E} + i\omega\mu_0 \underline{\sigma} \boldsymbol{E} = 0, \tag{34}$$

where the conductivity in the uniaxial anisotropy layer is

$$\underline{\sigma} = \begin{pmatrix} \sigma_{\parallel} & & \\ & \sigma_{\parallel} & \\ & & \sigma_{\perp} \end{pmatrix}, \tag{35}$$

and takes the z-component from the equation (30):

$$\partial_{xz} E_x - \partial_{xx} E_z - \partial_{yy} E_z + \partial_{yz} E_y + i\omega\mu\sigma_{\perp} E_z = 0. \tag{36}$$

This equation is effective inside the lower half-space (z>0) since the HED source is located in the upper half-space (z<0). The continuity equation [$\boldsymbol{\nabla}\left(\underline{\sigma}\boldsymbol{E}\right) = 0$], following Yu and Edwards (1992), is also applied to derive equation (6). To multiply ∂_z to the above continuity condition for the conductivity of uniaxial tensor, the continuity equation $\partial_z\left[\boldsymbol{\nabla}\left(\underline{\sigma}\boldsymbol{E}\right)\right] = 0$ is

$$\sigma_{\parallel} \partial_{xz} E_x + \sigma_{\parallel} \partial_{yz} E_y + \sigma_{\perp} \partial_{zz} E_z = 0. \tag{37}$$

To multiply $\sigma_{\parallel}$ to the equation (36), the result is

$$\sigma_{\parallel} \partial_{xz} E_x - \sigma_{\parallel} \partial_{xx} E_z - \sigma_{\parallel} \partial_{yy} E_z + \sigma_{\parallel} \partial_{yz} E_y + \sigma_{\parallel} i\omega\mu\sigma_{\perp} E_z = 0\,. \tag{38}$$

Substituting $\sigma_{\parallel}\partial_{xz}E_x + \sigma_{\parallel}\partial_{yz}E_y = -\sigma_{\perp}\partial_{zz}E_z$ from equation (37) into (38) for taking ∂_{xz} and ∂_{yz} components away, and divide by $\sigma_{\parallel}$, the final form of the PDE is derived as (5). This equation (5) can be solved by the application of a 2-D Fourier transform in the *x*- and *y*-directions. The second-order derivatives $\partial^2/\partial x^2$ and $\partial^2/\partial y^2$ in spatial domain match to multiplications in the wavenumber domain by $-p^2$ and $-q^2$,

$$\left(-\frac{\sigma_{\parallel}}{\sigma_{\perp}}p^2 - \frac{\sigma_{\parallel}}{\sigma_{\perp}}q^2 - i\omega\mu\sigma_{\parallel}\right)e_z + \frac{d^2e_z}{dz^2} = 0, \tag{39}$$

therefore, the ordinary differential equation (ODE) is derived such as equation (6).

Similarly, the ODE equation (7) can be derived by eliminating the electric field factor from equations (3) and (4).

$$\boldsymbol{\nabla} \times \boldsymbol{\nabla} \times \boldsymbol{B} + i\omega\mu_0\underline{\sigma}\boldsymbol{B} = 0; \tag{40}$$

$$\boldsymbol{\nabla} \times \underline{\sigma}^{-1}\boldsymbol{\nabla} \times \boldsymbol{B} + i\omega\mu_0\boldsymbol{B} = 0, \tag{41}$$

where the inverse of the electrical conductivity is

$$\underline{\sigma}^{-1} = \begin{pmatrix} {\sigma_{\parallel}}^{-1} & & \\ & {\sigma_{\parallel}}^{-1} & \\ & & {\sigma_{\perp}}^{-1} \end{pmatrix}. \tag{42}$$

The z-component of equation (40) is

$$\partial_{xz}B_x - \partial_{xx}B_z - \partial_{yy}B_z + \partial_{yz}B_y + i\omega\mu\sigma_{\perp}B_z = 0. \tag{43}$$

The divergence free condition of the magnetic field [$\boldsymbol{\nabla} \cdot \boldsymbol{B} = 0$] is applied and to multiply ∂_z to the above divergence free condition, then the result is

$$\partial_{xz}B_x + \partial_{yz}B_y + \partial_{zz}B_z = 0. \tag{44}$$

Likewise above electric field derivation, to substitute $\partial_{xz}B_x + \partial_{yz}B_y = -\partial_{zz}B_z$ from equation (44) into (43) to take ∂_{xz} and ∂_{yz} components away, the final form of the PDE is derived as

$$-\frac{\partial^2 B_z}{\partial x^2} - \frac{\partial^2 B_z}{\partial y^2} - \frac{\partial^2 B_z}{\partial z^2} + i\omega\mu\sigma_\perp B_z = 0. \tag{45}$$

This equation also can be solved with a 2-D Fourier transform in the x- and y-directions. The second-order derivatives $\partial^2/\partial x^2$ and $\partial^2/\partial y^2$ in spatial domain correspond to multiplications in the wavenumber domain by $-p^2$ and $-q^2$,

$$-(p^2 + q^2 + i\omega\mu\sigma_\perp)b_z + \frac{d^2 b_z}{dz^2} = 0, \tag{46}$$

therefore, the ODE is derived such as equation (7).

APPENDIX B

To find exact solutions to boundary value problems involving HED sources, it has proven convenient to use the Hertz vector (Π), in terms of the electromagnetic field E and B in conductors. The source terms to the x- and y-direction by the HED transmitter are already calculated (1990, 1999 Everett) for solving the vertically conductivity uniaxil model, however, the z-direction needs to be derive for solving in horizontally conductive uniaxil model. From the Sommerfeld (1964), double half-space fields can be attained from the following the Hertz vector;

$$\boldsymbol{B} = \mu_0 \sigma_i \nabla \times \boldsymbol{\Pi}; \tag{47}$$

$$\boldsymbol{E} = -i\mu_0 \sigma_i \omega \boldsymbol{\Pi} + \nabla(\nabla \cdot \boldsymbol{\Pi}). \tag{48}$$

Combining (7) and (8), we can obtain the diffusion equation obeyed by the Hertz vector

$$\nabla^2 \boldsymbol{\Pi} - i\mu_0 \sigma_i \omega \boldsymbol{\Pi} = \frac{\boldsymbol{J_s}}{\sigma_i}, \tag{49}$$

where $i=0$(seawater), 1(seafloor). The solutions of the Hertz vectors in each direction of double half-space already have obtained (Everett 1990), and the results are;

$$\Pi_x = \begin{cases} \Pi_x{}^{seawater} = \dfrac{P}{2\pi\sigma_0} \displaystyle\int_0^\infty \frac{exp\ (-u_0 z)}{u_0 + u_1} \lambda J_0(\lambda\rho) d\lambda & z > 0; \quad (50a) \\ \Pi_x{}^{seafloor} = \dfrac{P}{2\pi\sigma_1} \displaystyle\int_0^\infty \frac{exp\ (u_1 z)}{u_0 + u_1} \lambda J_0(\lambda\rho) d\lambda & z < 0, \quad (50b) \end{cases}$$

$$\Pi_y = \begin{cases} \Pi_y{}^{seawater} = 0 & z > 0; \quad (51a) \\ \Pi_y{}^{seafloor} = 0 & z < 0, \quad (51b) \end{cases}$$

$$\Pi_z = \begin{cases} \Pi_z{}^{seawater} = \dfrac{-P}{2\pi i\mu_0\sigma_0\omega}\dfrac{\partial}{\partial x}\displaystyle\int_0^\infty \frac{(u_0-u_1)exp\,(-u_0 z)}{\sigma_1 u_0+\sigma_0 u_1}\lambda J_0(\lambda\rho)d\lambda \quad z>0; (52a) \\ \Pi_z{}^{seafloor} = \dfrac{-P}{2\pi i\mu_0\sigma_1\omega}\dfrac{\partial}{\partial x^2}\displaystyle\int_0^\infty \frac{(u_0-u_1)exp\,(u_1 z)}{\sigma_1 u_0+\sigma_0 u_1}\lambda J_0(\lambda\rho)d\lambda \quad z>0, (52b) \end{cases}$$

where $J_0(\lambda\rho)$is a Bessel function of zero order, $\rho=\sqrt{x^2+y^2}$,

$u_i=\sqrt{\lambda^2+i\mu_i\omega\sigma_i}$, and $\lambda=\sqrt{p^2+q^2}$. The electric components of z-direction from equation (48) can be written in terms of the above Hertz vector components (50) ~ (52),

$$E_z = -i\mu_0\sigma_i\omega\Pi_z + \frac{\partial^2\Pi_x}{\partial x\partial z}+\frac{\partial^2\Pi_z}{\partial z^2} = E_z^{(1)}+E_z^{(2)}+E_z^{(3)}. \quad (53)$$

where $E_z^{(1)}=-i\mu_0\sigma_i\omega\Pi_z$, $E_z^{(2)}=\frac{\partial^2\Pi_x}{\partial x\partial z}$ and $E_z^{(3)}=\frac{\partial^2\Pi_z}{\partial z^2}$. With the chain rule $\frac{\partial\rho}{\partial x}=\frac{x}{\rho}$, and the Bessel function derivation, $\frac{\partial}{\partial x}J_0(\lambda\rho)=\frac{-\lambda x J_1(\lambda\rho)}{\rho}$, we can simplify E_z

$$E_z = \begin{cases} \dfrac{P}{2\pi}\displaystyle\int_0^\infty \lambda d\lambda\exp(-u_0 z)\left[\frac{(u_0-u_1)}{(\sigma_0 u_1+\sigma_1 u_0)}\frac{\partial}{\partial x}J_0(\lambda\rho)-\right. \\ \left.\dfrac{P}{2\pi}\displaystyle\int_0^\infty \lambda d\lambda\exp(u_1 z)\left[\frac{(u_0-u_1)}{\sigma_0 u_1+\sigma_1 u_0}\frac{\partial}{\partial x}J_0(\lambda\rho)+\right.\right. \\ \left.\left.\frac{u_0}{\sigma_0(u_1+u_0)}\frac{\partial}{\partial x}J_0(\lambda\rho)+\frac{1}{i\mu_0\sigma_0\omega}\frac{u_0(u_0-u_1)}{\sigma_0 u_1+\sigma_1 u_0}\frac{\partial^2}{\partial z^2}J_0(\lambda\rho)\right]; \quad (54a) \\ \left.\frac{u_0}{\sigma_1(u_1+u_0)}\frac{\partial}{\partial x}J_0(\lambda\rho)-\frac{1}{i\mu_0\sigma_1\omega}\frac{u_0(u_0-u_1)}{\sigma_0 u_1+\sigma_1 u_0}\frac{\partial^2}{\partial z^2}J_0(\lambda\rho)\right]. \quad (54b) \end{cases}$$

In wholespace, the conductivity $\sigma_i=\sigma_0=\sigma_1$, and $u_i=u_1=u_0$. Therefore, $E_z^{(1)}, E_z^{(3)}$ components are vanished. Now, we obtain the final form of E_z as function of the Bessel function of zero kind,

$$E_z = \begin{cases} \dfrac{-P}{4\pi\sigma}\displaystyle\int_0^\infty \lambda d\lambda \exp(-uz)\frac{\partial}{\partial x}J_0(\lambda\rho)\,; & (55a) \\ \dfrac{P}{4\pi\sigma}\displaystyle\int_0^\infty \lambda d\lambda \exp(uz)\frac{\partial}{\partial x}J_0(\lambda\rho)\,. & (55b) \end{cases}$$

The 2-D Fourier transform and its inverse form (eq. (1) ~ (2)) are also related to Hankel transform which is a form of Bessel function of zero order

$$\int_0^\infty d\lambda f(\lambda^2)\lambda\frac{\partial}{\partial x}J_0(\lambda\rho) = \frac{1}{2\pi}\int_{-\infty}^\infty\int_{-\infty}^\infty dpdq\; pf(p^2+q^2)\,exp(-ipx)exp(-iqy)\,; \quad (56)$$

$$\int_0^\infty d\lambda f(\lambda^2)\lambda\frac{\partial}{\partial x}J_0(\lambda\rho) = \frac{-i}{2\pi}\int_{-\infty}^\infty\int_{-\infty}^\infty dpdq\; pf(p^2+q^2)\,exp(-ipx)exp(-iqy). \quad (57)$$

The function $f(\lambda^2)$ can be defined in equation (56) and (57), and these equations have double Fourier transform. Thus, the function $f(\lambda^2)$ is

$$f(\lambda^2) = \begin{cases} \dfrac{-P}{4\pi\sigma}exp(-uz)\,; & (58a) \\ \dfrac{P}{4\pi\sigma}exp(uz)\,. & (58b) \end{cases}$$

Replacing function (58) to the equation (57), gives the desired result:

$$E_z = \begin{cases} \dfrac{-i}{2\pi}\displaystyle\int_{-\infty}^\infty\int_{-\infty}^\infty \frac{-pP}{4\pi\sigma}exp(-uz)\,exp(-ipx)\,exp(-iqy)\,dp\,dq\,; & (59a) \\ \dfrac{-i}{2\pi}\displaystyle\int_{-\infty}^\infty\int_{-\infty}^\infty \frac{pP}{4\pi\sigma}exp(uz)\,exp(-ipx)\,exp(-iqy)\,dp\,dq\,; & (59b) \end{cases}$$

$$E_z = \begin{cases} \dfrac{iP}{8\pi^2\sigma}\displaystyle\int_{-\infty}^\infty\int_{-\infty}^\infty p\,exp(-uz)\,exp(-ipx)\,exp(-iqy)\,dp\,dq\,; & (59c) \\ \dfrac{-iP}{8\pi^2\sigma}\displaystyle\int_{-\infty}^\infty\int_{-\infty}^\infty p\,exp(uz)\,exp(-ipx)\,exp(-iqy)\,dp\,dq\,. & (59d) \end{cases}$$

These above expression may be more simplified. The exponential components are changed the cosine and sine, and the pair of terms in the above are even function of p, thus the formula are

$$E_z = \begin{cases} \frac{iP}{4\pi^2\sigma}\int_{-\infty}^{\infty} dp \int_0^{\infty} dq\ p\ exp(-uz)\ cos\ qy\ exp(-ipx)\ ; & (60a) \\ \frac{-iP}{4\pi^2\sigma}\int_{-\infty}^{\infty} dp \int_0^{\infty} dq\ p\ exp(uz)\ cos\ qy\ exp(-ipx)\,. & (60b) \end{cases}$$

Also, the pairs of terms in the above are odd function in q, thus the final forms of E_z are

$$E_z = \begin{cases} \frac{P}{2\pi^2\sigma}\int_0^{\infty}\int_0^{\infty} dp\ dq\ p \exp(-uz) \cos qy \sin px\ ; & (61a) \\ \frac{-P}{2\pi^2\sigma}\int_0^{\infty}\int_0^{\infty} dp\ dq\ p \exp(uz) \cos qy \sin px. & (61b) \end{cases}$$

Receivers are below the distance h from the dipole, so we plug h into z to -h, thus,

$$E_z = \frac{-P}{2\pi^2\sigma}\int_0^{\infty}\int_0^{\infty} dp\ dq\ p\ exp(uz) \cos qy \sin px\ ; \quad (62a)$$

$$E_z = \frac{1}{\pi^2}\int_0^{\infty}\int_0^{\infty} dp\ dq\ \left[\frac{-pP}{2\sigma} exp(-uh)\right] \cos qy \sin px\ . \quad (62b)$$

Now, equation (62b) is the integral of double sine and cosine in p, q domain. Thus, the source term of electric field from HED dipole in z-direction is

$$_1 = \frac{-pP}{2\sigma} exp(-uh). \quad (63)$$

Likewise, the source term of magnetic field due to HED dipole in z-direction is derived from equation (48). Magnetic field is defined as form of Hertz vector

$$B_z = \mu_0\sigma_i \frac{\partial \Pi_y}{\partial x} - \mu_0\sigma_i \frac{\partial \Pi_x}{\partial y} = B_z^{(1)} + B_z^{(2)}. \quad (64)$$

where $B_z^{(1)} = \mu_0 \sigma_i \frac{\partial \Pi_y}{\partial x}$, $B_z^{(2)} = -\mu_0 \sigma_i \frac{\partial \Pi_x}{\partial y}$. With the chain rule $\frac{\partial \rho}{\partial y} = \frac{y}{\rho}$, and the Bessel function derivation, $\frac{\partial}{\partial y} J_0(\lambda\rho) = \frac{-\lambda y J_1(\lambda\rho)}{\rho}$, we can simplify B_z as

$$B_z = \begin{cases} \frac{-\mu_0 P}{2\pi} \int_0^\infty \frac{exp\ (-uz)}{2u} \lambda \frac{\partial}{\partial y} J_0(\lambda\rho) d\lambda\,; & (65a) \\ \frac{-\mu_0 P}{2\pi} \int_0^\infty \frac{exp\ (uz)}{2u} \lambda \frac{\partial}{\partial y} J_0(\lambda\rho) d\lambda\,. & (65b) \end{cases}$$

The function $f(\lambda^2)$ can be defined in equation (61), and these equations have double Fourier transform. Thus, the function $f(\lambda^2)$ is

$$f(\lambda^2) = \begin{cases} \frac{-\mu_0 P}{4\pi u} ex\,p(-uz)\,; & (66a) \\ \frac{-\mu_0 P}{4\pi u} ex\,p(uz)\,. & (66b) \end{cases}$$

Applying equation (61) to the equation (62), gives the desired result

$$B_z = \begin{cases} \frac{-i}{2\pi} \int_{-\infty}^\infty \int_{-\infty}^\infty \frac{-\mu_0 q P}{4\pi u} ex\,p(-uz)\, exp(-ipx)\, ex\,p(-iqy)\, dp\, dq\,; & (67a) \\ \frac{-i}{2\pi} \int_{-\infty}^\infty \int_{-\infty}^\infty \frac{-\mu_0 q P}{4\pi u} exp\ (uz)\, exp(-ipx)\, exp\ (-iqy) dp\, dq\,, & (67b) \end{cases}$$

$$B_z = \begin{cases} \frac{i\mu_0 P}{8\pi^2 u} \int_{-\infty}^\infty \int_{-\infty}^\infty q exp\ (-uz)\, exp(-ipx)\, exp\ (-iqy) dp\, dq\,; & (67c) \\ \frac{i\mu_0 P}{8\pi^2 u} \int_{-\infty}^\infty \int_{-\infty}^\infty q exp\ (uz)\, exp(-ipx)\, exp\ (-iqy) dp\, dq\,. & (67d) \end{cases}$$

These above expression also may be more simplified. The exponential components are changed the cosine and sine, ant the pairs of terms in the above are even function of q, thus the formula

$$B_z = \begin{cases} \dfrac{\mu_0 P}{4\pi^2 u} \int_{-\infty}^{\infty} \int_{0}^{\infty} q\ exp\ (-uz)\ exp(-ipx)\ sin\ qy\ dp\ dq\ ; & (68a) \\ \dfrac{\mu_0 P}{4\pi^2 u} \int_{-\infty}^{\infty} \int_{0}^{\infty} q\ exp\ (uz)\ exp(-ipx)\ sin\ qy\ dp\ dq\ . & (68b) \end{cases}$$

Also, the pairs of terms in the above are odd function in p, thus the final form of B_z is

$$B_z = \begin{cases} \dfrac{\mu_0 P}{2\pi^2 u} \int_{0}^{\infty} \int_{0}^{\infty} q \exp(-uz)\ sin\ qy\ cos\ px\ dp\ dq\ ; & (69a) \\ \dfrac{\mu_0 P}{2\pi^2 u} \int_{0}^{\infty} \int_{0}^{\infty} q \exp(uz)\ sin\ qy\ cos\ px\ dp\ dq\ . & (69b) \end{cases}$$

Receivers are below the distance h from the dipole, so we plug h into z to -h, thus,

$$B_z = \frac{1}{\pi^2} \int_{0}^{\infty} \int_{0}^{\infty} \frac{\mu_0 qP}{2u} exp\ (uz) \sin \text{qy} \cos \text{px}\, dp\ dq\ ; \quad (70a)$$

$$B_z = \frac{1}{\pi^2} \int_{0}^{\infty} \int_{0}^{\infty} dp\ dq\ \left[\frac{\mu_0 qP}{2u} exp(uz)\right] sin\ qy\ cos\ px\ . \quad (70\text{b})$$

Now, equation (70b) is the integral of double sine and cosine in p, q domain. Thus, the source term of electric filed from HED dipole in z-direction is

$$_2 = \frac{\mu_0 qP}{2u} exp(-uh). \quad (71)$$

APPENDIX C

In this part, the final forms of e_x, b_x, e_y, b_y are derived from e_z, b_z components to make boundary conditions at each interface. The equations (14) and (15) can be converted (p, q) wavenumber domains by 2-D Fourier transform. Each component of *x*-, *y*- and *z*-direction of equation (14) is expressed by:

$$iqe_z - \partial_z e_y = -iwb_x; \tag{72}$$

$$\partial_z e_x - ipe_z = -iwb_y; \tag{73}$$

$$ipe_y - iqe_x = -iwb_z, \tag{74}$$

and each component of *x*-, *y*- and *z*-direction of equation (15) is also expressed by:

$$iqb_z - \partial_z b_y = \mu\sigma_{\parallel} e_x; \tag{75}$$

$$\partial_z b_x - ipb_z = \mu\sigma_{\parallel} e_y; \tag{76}$$

$$ipb_y - iqb_x = \mu\sigma_{\perp} e_z. \tag{77}$$

To derive e_x, b_x, e_y, b_y as a function of e_z, b_z which was already solved by equations (8) ~ (13), these are accomplished by the following manipulations of equations (72) ~ (77) with the divergence free condition of magnetic field [$\boldsymbol{\nabla} \cdot \boldsymbol{b} = 0$] and the continuity equation [$\boldsymbol{\nabla}\left(\underline{\sigma}\boldsymbol{e}\right) = 0$] of electric field as a form of wavenumber domain:

$$ip\sigma_{\parallel} e_x + iq\sigma_{\parallel} e_y + \partial_z \sigma_{\perp} e_z = 0; \tag{78}$$

$$ipb_x + iqb_y + \partial_z b_z = 0. \tag{79}$$

Multiplying $\sigma_{\parallel} q$ to equation (74) and multiplying p to equation (78), and then subtracting each equation to eliminate e_y component, the result is

$$e_x = \frac{1}{\sigma_{\parallel}(p^2+q^2)}(ip\partial_z\sigma_{\perp}e_z + w\sigma_{\parallel}qb_z). \tag{80}$$

Likewise, multiplying $\sigma_{\parallel}p$ to equation (74) and multiplying q to equation (78), and then subtracting each equation to eliminate e_x component, the result is

$$e_y = \frac{1}{\sigma_{\parallel}(p^2+q^2)}(iq\partial_z\sigma_{\perp}e_z - w\sigma_{\parallel}pb_z)\,. \tag{81}$$

Multiplying q to equation (77) and multiplying p to equation (79), and then subtracting each equation to eliminate b_y component, the result is

$$b_x = \frac{i}{p^2+q^2}(p\partial_z b_z + q\mu\sigma_{\perp}e_z). \tag{82}$$

Likewise, multiplying p to equation (77) and multiplying q to equation (79), and subtracting each equation to eliminate b_x component, the result is

$$b_y = \frac{i}{p^2+q^2}(q\partial_z b_z - p\mu\sigma_{\perp}e_z). \tag{83}$$

APPENDIX D

The boundary conditions at each interface yield 8 unknown coefficients (A-H) in equation (8) ~ (13). The tangential EM field components (e_x, b_x, e_y, b_y) must be continuous at each interface. The e_x, b_x, e_y, b_y components are expressed by e_z, b_z components in equation (80) ~ (83). The electrical conductivity of seawater is $\sigma_\perp = \sigma_\parallel = \sigma_w = \sigma_0$, and the electrical conductivity of isotropy layer is $\sigma_\perp = \sigma_\parallel = \sigma_3$ in Figure 4. Thus, the e_x components at each layer are:

$$e_x^0 = \frac{1}{(p^2+q^2)}(i\partial_z p e_z^0 + wqb_z^0); \tag{84}$$

$$e_x^1 = \frac{1}{\sigma_\parallel(p^2+q^2)}(i\partial_z \sigma_\perp p e_z^1 + w\sigma_\parallel q b_z^1); \tag{85}$$

$$e_x^2 = \frac{1}{(p^2+q^2)}(i\partial_z p e_z^2 + wqb_z^2). \tag{86}$$

Likewise, the e_y components at each layer are:

$$e_y^0 = \frac{1}{(p^2+q^2)}(i\partial_z q e_z^0 - wpb_z^0); \tag{87}$$

$$e_y^1 = \frac{1}{\sigma_\parallel(p^2+q^2)}(i\partial_z \sigma_\perp q e_z^1 - w\sigma_\parallel p b_z^1); \tag{88}$$

$$e_y^2 = \frac{1}{(p^2+q^2)}(i\partial_z q e_z^2 - wpb_z^2). \tag{89}$$

The b_x components at each layer are:

$$b_x^0 = \frac{i}{p^2+q^2}(p\partial_z b_z^0 + \mu\sigma_w q e_z^0); \tag{90}$$

$$b_x^1 = \frac{i}{p^2+q^2}(p\partial_z b_z^1 + \mu\sigma_\perp q e_z^1); \tag{91}$$

$$b_x^2 = \frac{i}{p^2+q^2}(p\partial_z b_z^2 + \mu\sigma_3 q e_z^2). \tag{92}$$

Finally, the b_y components at each layer are:

$$b_y^0 = \frac{i}{p^2+q^2}(q\partial_z b_z^0 - \mu\sigma_w p e_z^0); \tag{93}$$

$$b_y^1 = \frac{i}{p^2+q^2}(q\partial_z b_z^1 - \mu\sigma_\perp p e_z^1); \tag{94}$$

$$b_y^2 = \frac{i}{p^2+q^2}(q\partial_z b_z^2 - \mu\sigma_3 p e_z^2). \tag{95}$$

The source terms Γ_1 and Γ_2 are already solved in Appendix B. These equations (84) ~ (95) have to satisfy continuous at each interface boundary. Thus, at the interface I, which is seafloor, the continuous are $e_x^0 = e_x^1$, $e_y^0 = e_y^1$, $b_x^0 = b_x^1$, $b_y^0 = b_y^1$. Likewise, at the interface II, which is boundary between an anisotropic and an isotropic layer, the continuous relationships are $e_x^1 = e_x^2$, $e_y^1 = e_y^2$, $b_x^1 = b_x^2$, $b_y^1 = b_y^2$. Final results are below.

On condition that $e_x^0 = e_x^1$;

$$iu_0\sigma_\parallel pA + w\sigma_\parallel qB + iu_2\sigma_\perp pC - iu_2\sigma_\perp pD - w\sigma_\parallel qE - w\sigma_\parallel qF = iu_0\sigma_\parallel p\Gamma_1 - w\sigma_\parallel q\Gamma_2. \tag{96}$$

On condition that $e_y^0 = e_y^1$;

$$iu_0\sigma_\parallel qA - w\sigma_\parallel pB + iu_2\sigma_\perp qC - iu_2\sigma_\perp qD + w\sigma_\parallel pE + w\sigma_\parallel pF = iu_0\sigma_\parallel q\Gamma_1 + w\sigma_\parallel p\Gamma_2. \tag{97}$$

On condition that $b_x^0 = b_x^1$;

$$\mu\sigma_w qA + pu_0 B - \mu\sigma_\perp qC - \mu\sigma_\perp qD + pu_1 E - pu_1 F = pu_0\Gamma_2 - \mu\sigma_w q\Gamma_1. \quad (98)$$

On condition that $b_y^0 = b_y^1$;

$$\mu\sigma_w pA - qu_0 B - \mu\sigma_\perp pC - \mu\sigma_\perp pD - qu_1 E + qu_1 F = -qu_0\Gamma_2 - \mu\sigma_w p\Gamma_1. \quad (99)$$

On condition that $e_x^1 = e_x^2$;

$$-iu_2\sigma_\perp p\, exp(-u_2 d)\, C + iu_2\sigma_\perp p\, exp(u_2 d) D + w\sigma_\perp q\, exp(-u_1 d)\, E$$
$$+w\sigma_\parallel q\, exp(u_1 d)\, F + iu_3\sigma_\parallel p\, exp(-u_3 d)\, G - w\sigma_\parallel q\, exp(-u_3 d)\, H = 0. \quad (100)$$

On condition that $e_y^1 = e_y^2$;

$$-iu_2\sigma_\perp q\, exp(-u_2 d)\, C + iu_2\sigma_\perp q\, exp(u_2 d)\, D - w\sigma_\parallel p\, exp(-u_1 d)\, E$$
$$-w\sigma_\parallel p\, exp(u_1 d)\, F + iu_3\sigma_\parallel q\, exp(-u_3 d)\, G + w\sigma_\parallel p\, exp(-u_3 d)\, H = 0. \quad (101)$$

On condition that $b_x^1 = b_x^2$;

$$\mu\sigma_\perp q\, exp(-u_2 d)\, C + \mu\sigma_\perp q\, exp(u_2 d)\, D - pu_1\, exp(-u_1 d)\, E + pu_1\, exp(u_1 d)\, F$$
$$-\mu\sigma_3 q\, exp(-u_3 d)\, G + pu_3\, exp(-u_3 d)\, H = 0. \quad (102)$$

On condition that $b_y^1 = b_y^2$;

$$\mu\sigma_\perp p\, exp(-u_2 d)\, C + \mu\sigma_\perp p\, exp(u_2 d)\, D + qu_1\, exp(-u_1 d)\, E - qu_1\, exp(u_1 d)\, F$$
$$-\mu\sigma_3 p\, exp(-u_3 d)\, G - qu_3\, exp(-u_3 d)\, H = 0. \quad (103)$$

There are 8 unknown coefficients and 8 linear equations, thus, these equations can be solved by linear algebra, as AX = B, where A is 8 by 8 matrix, X is 8 by 1 matrix, and B is 8 by 1 matrix. The total matrix is below;

$$\begin{pmatrix} iu_0\sigma_{\parallel}p & w\sigma_{\parallel}q & iu_2\sigma_{\perp}p & -iu_2\sigma_{\perp}p & -w\sigma_{\parallel}q & -w\sigma_{\parallel}q & 0 & 0 \\ iu_0\sigma_{\parallel}q & -w\sigma_{\parallel}p & iu_2\sigma_{\perp}q & -iu_2\sigma_{\perp}q & w\sigma_{\parallel}p & w\sigma_{\parallel}p & 0 & 0 \\ \mu\sigma_w q & pu_0 & -\mu\sigma_{\perp}q & -\mu\sigma_{\perp}q & pu_1 & -pu_1 & 0 & 0 \\ \mu\sigma_w p & -qu_0 & -\mu\sigma_{\perp}p & -\mu\sigma_{\perp}p & -qu_1 & qu_1 & 0 & 0 \\ 0 & 0 & -iu_2\sigma_{\perp}p\,exp(-u_2d) & iu_2\sigma_{\perp}p\,exp(u_2d) & w\sigma_{\parallel}q\,exp(-u_1d) & w\sigma_{\parallel}q\,exp(u_1d) & iu_3\sigma_{\parallel}p\,exp(-u_3d) & -w\sigma_{\parallel}q\,exp(-u_3d) \\ 0 & 0 & -iu_2\sigma_{\perp}q\,exp(-u_2d) & iu_2\sigma_{\perp}q\,exp(u_2d) & -w\sigma_{\parallel}p\,exp(-u_1d) & -w\sigma_{\parallel}p\,exp(u_1d) & iu_3\sigma_{\parallel}q\,exp(-u_3d) & w\sigma_{\parallel}p\,exp(-u_3d) \\ 0 & 0 & \mu\sigma_{\perp}q\,exp(-u_2d) & \mu\sigma_{\perp}q\,exp(u_2d) & -pu_1\,exp(-u_1d) & pu_1\,exp(u_1d) & -\mu\sigma_3 q\,exp(-u_3d) & pu_3\,exp(-u_3d) \\ 0 & 0 & \mu\sigma_{\perp}p\,exp(-u_2d) & \mu\sigma_{\perp}p\,exp(u_2d) & qu_1\,exp(-u_1d) & -qu_1\,exp(u_1d) & -\mu\sigma_3 p\,exp(-u_3d) & -qu_3\,exp(-u_3d) \end{pmatrix} \begin{pmatrix} A \\ B \\ C \\ D \\ E \\ F \\ G \\ H \end{pmatrix}$$

$$= \begin{pmatrix} iu_0\sigma_{\parallel}p\Gamma_1 - w\sigma_{\parallel}q\Gamma_2 \\ iu_0\sigma_{\parallel}q\Gamma_1 + w\sigma_{\parallel}p\Gamma_2 \\ -\mu\sigma_w q\Gamma_1 + pu_0\Gamma_2 \\ -\mu\sigma_w p\Gamma_1 - qu_0\Gamma_2 \\ 0 \\ 0 \\ 0 \\ 0 \end{pmatrix} \quad (104)$$